American Journal of Mechanical Engineering, 2019, Vol. 7, No. 2, 87-106
Available online at http://pubs.sciepub.com/ajme/7/2/5
Published by Science and Education Publishing
DOI:10.12691/ajme-7-2-5

Influence of Multi-Level Printing Process Parameters on 3D Printed Parts in Fused Deposition Molding of Poly(lactic) Acid Plus: A Comprehensive Investigation

Mohammad S. Alsoufi*, Mohammed W. Alhazmi, Dhia K. Suker, Wadeea K. Hafiz, Sultan S. Almalki, Rashad O. Malibari

Department of Mechanical Engineering, College of Engineering and Islamic Architecture, Umm Al-Qura University, Makkah, KSA
*Corresponding author: mssoufi@uqu.edu.sa

Received March 03, 2019; Revised May 04, 2019; Accepted May 13, 2019

Abstract This research paper presents results of a study evaluating the influence of multi-level printing process parameters on 3D printed parts in FDM of PLA Plus. In this study, the effects of printing temperature, printing speed along with skirt/brim with and without top/bottom thickness were considered. The investigations show that the measured dimensions are always more than the CAD dimension along the *z*-direction (height) but dimensions along *x*- and *y*-directions (length and width) are less than the CAD dimension and not necessarily equal. The surface roughness fluctuated over independent printing process parameters along with the density. The results show that the Q-Q (quantile-quantile) plot of density is a very impressive and promising method in 3D FDM printing process parameters optimization.

Keywords: *surface roughness, density, FDM, PLA plus, skirt, brim*

Cite This Article: Mohammad S. Alsoufi, Mohammed W. Alhazmi, Dhia K. Suker, Wadeea K. Hafiz, Sultan S. Almalki, and Rashad O. Malibari, "Influence of Multi-Level Printing Process Parameters on 3D Printed Parts in Fused Deposition Molding of Poly(lactic) Acid Plus: A Comprehensive Investigation." *American Journal of Mechanical Engineering*, vol. 7, no. 2 (2019): 87-106. doi: 10.12691/ajme-7-2-5.

1. Introduction

Three-dimensional (3D) printing technology belongs to the emerging topics and issues of our real-time. On the one hand, allowing both localization and individualization of manufacturing production on demand [1], on the other hand, non-traditional (non-conventional) machining offers new materials along with innovation in order to fabricate three-dimensional (3D) printing objects that would have been extremely difficult or near impossible with former technologies [2,3]. Rapid manufacturing (RM) technology (also known as additive manufacturing) is the latest approach for the additive fabrication (AF) technique that is used for manufacturing end-use solid items in a layer-by-layer or path-by-path procedure directly from a digital CAD file (computer-aided design) [4,5], as opposed to other procedures such as traditional (conventional) material removal or material deformation [6]. It is significantly human invention mainly meant to deal with increased free-market competition in an integrated world economy that has resulted mainly in the requirement for manufacturers to speed up order-to-delivery in a continuous-improvement cycle of new customized products more frequently than ever before to meet customer-oriented concept demands [4,6]. With the growing complexity of product innovation, rapid prototyping (RP) technologies are gaining more widespread acceptance and global industrial sector demand is driving manufacturers in general to enhance and update the specifications quality with little tolerance equal to ±0.1 mm overall of each piece of RP equipment [7]. Additive manufacturing (AM) has been usefully adapted in several industries over the span of more than twenty years including medical [8], automotive, aerospace [9], machinery, and architecture industries [10,11,12,13]. Main AM systems are fused deposition molding (FDM) [13], stereolithography (SL) [14], laminated object manufacturing (LOM) [15], selective laser sintering (SLS) [16] and laser engineered net shaping (LENS) [17]. One of the most widely used technologies for 3D printing compared to others competing for dimensional printing technologies is fused deposition modeling (FDM) [18,19,20,21,22] and it is this which is predicted as a sustainable modern manufacturing platform for functional and structural products and also for industrial and house-use [23].

1.1. Fused Deposition Melding (FDM^{TM}) Technique

Fused deposition modeling (FDM) is one of most sophisticated rapid prototyping (RP) technologies available that is presently attracting attention [24]. It is based on

Cartesian configuration, which has *x*, *y* and *z*-axes for front to back motion and vice versa, left to right motion and vice versa and up to down motion and vice versa, [25] as shown in Figure 1. FDM is additive manufacturing (AM) technology trademarked by Stratasys during the 1980s [26]. It is generally used for 3D modeling systems, practical rapid prototyping methods and production applications in the manufacturing of custom-made parts. The main parts of the FDM machine include a filament feed mechanism, a heated liquefier chamber and a print head, gantry and build platform surface [27]. In FDM technique (the most common and the cheapest method), a heated nozzle precisely extrudes a printing engineering thermoplastic filament material (i.e., polylactic acid). Like other new rapid prototyping (RP) machines, one single layer (one single path) at a time is printed in a writing mode but typically the engineering thermoplastic filament material is immediately deposited on a build platform surface in order to obtain the desired 3D physical model (CAD models). Extrusion through a small nozzle diameter (depending on the selected material) resulting in a three-dimensional printed cylindrical coiled shape of each layer (path) with a much larger width compared to the small nozzle diameter [28]. Technically, the nozzle diameter can affect layer height and path width (i.e., the nozzle of bigger diameter extrudes thicker strings, and vice versa). Commercially, the heating element/chamber of the available FDM 3D machine has a maximum operating temperature of around 300°C, which indicates that the high melting point of thermoplastic filament materials cannot be processed using FDM 3D technology [29].

Principally, it works by converting a pre-existing CAD design software digital file into G-code for 3D printing to construct real-life 3D objects of any size by adding a successively complete layer of molten or semi-liquid thermoplastic filament material. In the printing state, the thermoplastic filament material is pushed directly through a long tube (called a "Bowden tube") into the hot-end with a precise temperature-controlled 3D printing nozzle (temperature used for printing) having a specific diameter at a pre-adjusted printing constant speed (including infill, wall, outer, inner and initial layer speeds) over a precise temperature-controlled building platform (temperature used for the heated build plate). Based on the actual dimensions of the 3D object (i.e., length, width, height, diameter, and so on), the heated printer extruder moves horizontally across the *x*-*y* plane in a precise pattern (identified by the 3D object shape) producing the first layers on the build platform surface. Successively complete layers (paths) are printed by either moving the heated nozzle or moving the build platform surface through the *z*-plane with a precise distance equal to the layer height. The extruded thermoplastic filament material is solidified and cold welded onto the previous layer or path in approximately 0.1 seconds. Typically, the precise temperature-controlled nature of the build platform surface is lower than that of the extrusion head allowing the FDM 3D printed thermoplastic filament material to solidify quickly between each layer (each path) either naturally simultaneously or by help [26,30].

Figure 1. Cartesian configuration (square stage), adapted from [31]

1.2. Main Assumption and Contribution

Fused deposition modeling (FDM) is an AM technology that suffers seriously from poor surface roughness quality and geometry variation which require

hand finishing methods for even the necessary stages of printed part quality. In the literature review, a wide variety of approaches has addressed the problem of dimensional accuracy [32,33] and improving the surface roughness [34,35] of rapid prototyping printed parts. So, the current research work motivation is to experimentally reduce error in geometry variation (length, width and height) and surface roughness (R_a, R_q, R_{sk}, R_{ku} and R_q/R_a) and density (weight and volume) in a large number of printed parts. The authors establish decision criteria and design samples based on considerations of the geometry, surface roughness and density. The obtained results will be evaluated in such a way that they can be used for further employment in precision design and engineering materials development of FDM 3D printed components.

2. Experimental Work

2.1. Materials and Filament Extrusion

A commercially 1.75 mm diameter and tolerance of only ±0.02 mm of PLA Plus ($C_2H_4O_2$) were employed as the printing material. PLA Plus is a 100% biodegradable thermoplastic filament material derived from corn starch (a renewable resource), ten times stronger than regular PLA on the global market, without wire-drawing problems, no cracking and brittle issues, low surface roughness, low shrinkage rate filament material and uniform diameter. The thermoplastic filament material was purchased from eSUN which was initially founded in Shenzhen and used during the investigation. PLA Plus is an ideal material for prototypes (the actual scale systems) and models (the laboratory scale systems) that require aesthetic detail and eco-friendliness for both house-use and office-use [36]. The thermoplastic filament material was used as received.

2.2. FDM 3D Printer

For the printing process, the single extruder FDM 3D printer used in this study was based on an open-source low-cost desktop model known as Original Prusa I3 MK3 (purchased from PRUSA RESEARCH, Prague, Czech Republic). The FDM 3D system was used with a 0.4 mm nozzle diameter able to layer a height of 40 µm.

2.3. FDM 3D Dimension and Software

At the computer level, two professional forms of software were used in this study (Autodesk® Inventor Professional 2019 and Ultimaker Cura® 2019). The computer-aided design (CAD) design was drawn and visualized in Autodesk® Inventor Professional 2019 software (3D shape with 15 mm in length, 15 mm in width and 5 mm in height) as shown in Figure 2 and transferred to the 3D printable format using the Cura® software (open-source software) as shown in Figure 3. The Ultimaker Cura® 3.6 edition (www.ultimaker.com) was used to generate the machine code for the end-user FDM 3D printer from the 3D model (CAD model) file. One hundred samples were chosen for the final assessment.

Similarly, to many other AM systems, the FDM 3D system starts with a CAD file (generally in Standard Tessellation Language (STL) format). This digital CAD file is used to generate the cross-profile (the slices) that will be printed using FDM technology layer-by-layer (or path-by-path). The digital CAD file gives the layer's outline, being the software (i.e., Ultimaker Cura® 2019) used responsibly for defining the infill density settings of each layer (each path), setting the plot and path that the nozzle will follow. The general Marlin G-code for starting and ending the command is shown below with explanations for each line as comments.

Start G-code

```
G21 ; set units to millimeters
G90 ; use absolute positioning
M82 ; absolute extrusion mode
M104 S{material_print_temperature_layer_0} ; set extruder temp
M140 S{material_bed_temperature_layer_0} ; set bed temp
M190 S{material_bed_temperature_layer_0} ; wait for bed temp
M109 S{material_print_temperature_layer_0} ; wait for extruder temp
G28 W ; home all without mesh bed level
G80 ; mesh bed leveling
G92 E0.0 ; reset extruder distance position
G1 Y-3.0 F1000.0 ; go outside print area
G1 X60.0 E9.0 F1000.0 ; intro line
G1 X100.0 E21.5 F1000.0 ; intro line
G92 E0.0 ; reset extruder distance position
```

(1)

End G-code

```
M104 S0 ; turn off extruder
M140 S0 ; turn off heatbed
M107 ; turn off fan
G1 X0 Y210; home X axis and push Y forward
M84 ; disable motors
```

(2)

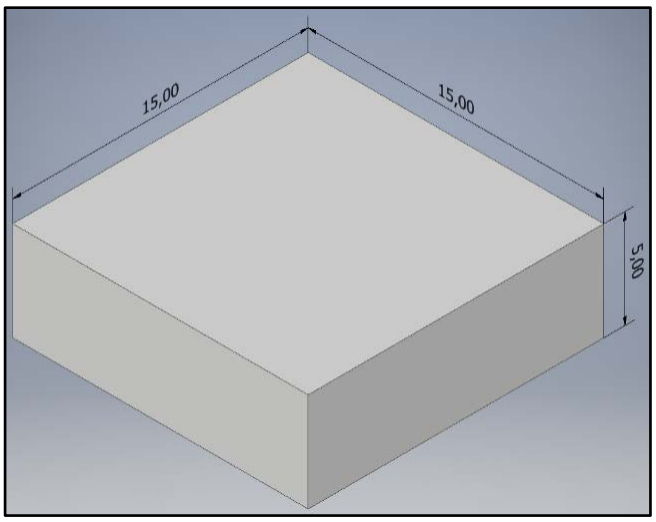

Figure 2. 3D physical shape

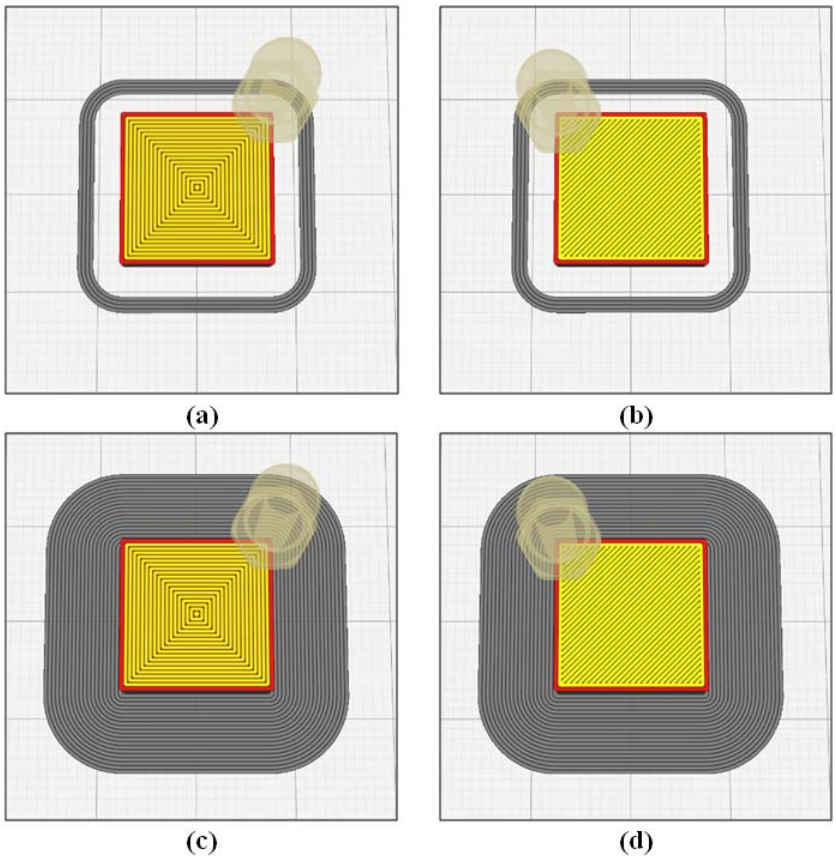

Figure 3. Cura software using 100% infill density of PLA Plus (a) skirt without top/bottom thickness, (b) skirt with top/bottom thickness, (c) brim without top/bottom thickness and (d) brim with a top/bottom thickness

2.4. FDM 3D Printing Process Parameters

Several printing runs were first completed in order to determine the best/optimal printing process parameters with PLA Plus. So, printing parameters were adopted by experimental values. Table 1 shows the comprehensive outlines of the FDM 3D process parameters used throughout the experiment. Other factors were maintained at their default levels as stated in Cura software.

With the multi-level process parameters used here, four independent levels were assessed namely “skirt without top/bottom thickness”, “skirt with top/bottom thickness”, “brim without top/bottom thickness” and “brim with top/bottom thickness”. Besides, five independent printing temperatures, T, 205°C, 210°C, 215°C, 220°C and 225°C were considered and recommended by the FDM 3D printer manufacturer. Furthermore, five independent printing speeds, v, 30 mm/s, 60 mm/s, 90 mm/s, 120 mm/s and 150 mm/s were also considered. Certain parameters such as layer height, wall thickness, infill density, infill pattern and printing direction were xed for all the printed samples in order to focus on the inuence of the previous process parameters. The inll pattern takes discrete string values. The Cura software is capable of implementing more than twelve different inll pattern types but, here only the concentric pattern was used for the optimization. A

drawing of the concentric pattern is shown in Figure 4. FDM 3D printed parts with the machine's minimum layers' height setting of 40 µm for a better surface quality finish. Regarding concern about the strength of the printed parts, infill density for FDM 3D printed parts are chosen at the highest responsible level (100% infill density). It is noted that there are other manufacturing process parameters set by Cura software and also that most parameters are configuration related parameters and do not affect the properties of the manufactured printed parts.

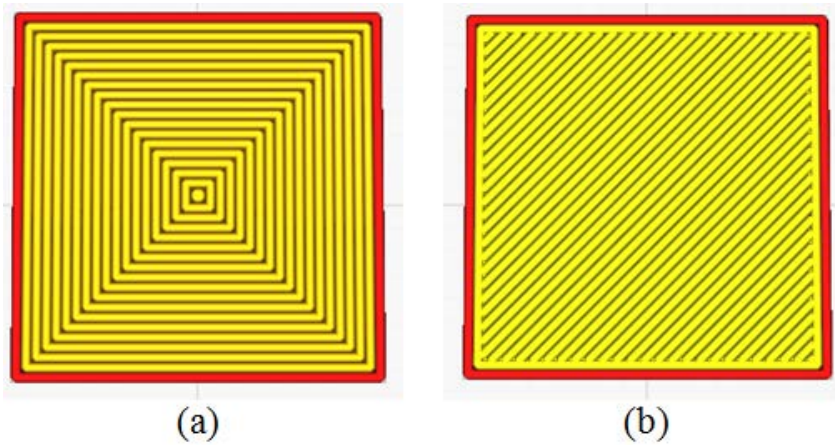

Figure 4. Concentric pattern with 100% infill (a) without top/bottom thickness (b) with a top/bottom thickness

Table 1. Printing process parameters and their levels used in this work

Setting	Parameters	Unit	Values				
Quality	Layer Height	mm	0.04				
Shell	Wall Thickness	mm	0.4				
	Wall Line Count	-	1				
	Top/Bottom Thickness (mm)	mm	0			0.6	
	Top Thickness	mm				0.6	
	Top Layer	-				2	
	Bottom Thickness	mm				0.6	
	Bottom Layer	-				2	
Infill	Infill Density	%	100				
	Infill Pattern	-	Concentric				
	Infill Line Direction	°	-				
	Infill Overlap Percentage	%	25				
	Infill Layer Thickness	mm	0.1				
Nozzle	Nozzle Size	mm	0.4				
	Compatible Material Diameter	mm	1.75				
	Nozzle Offset *x*-axis	mm	0				
	Nozzle Offset *y*-axis	mm					
Material	Filament Type	-	PLA Plus				
	Filament Colour	-	Grey	Brown	Green	Yellow	
	AM Process	-	FDM (Fused Deposition Modeling)				
	Printing Direction	-	Flat on Platform (on Printing Table)				
	Printing Temperature	°C	205	210	215	220	225
	Printing Temperature Initial Layer	°C					
	Initial Printing Temperature	°C					
	Final Printing Temperature	°C					
	Build Plate Temperature	°C	70				
	Build Plate Temperature Initial Layer	°C					
	Flow	%	100				
	Initial Layer Flow	%					
	Retraction Distance	mm	0.8				
	Retraction Speed	mm/s	35				
Speed	Print Speed	mm/s	30	60	90	120	150
	Infill Speed	mm/s					
	Wall Speed	mm/s	15	30	45	60	75
	Outer Wall Speed	mm/s					
	Inner Wall Speed	mm/s	30	60	90	120	150
	Top/Bottom Speed	mm/s	15	30	45	60	75
	Initial Layer Sped	mm/s					
Cooling	Fan Speed (%)	%	100				
Build Plate Adhesion	Build Plate Adhesion Type	-	Skirt			Brim	
	Skirt Lin Count	-	1			-	
	Skirt Distance	mm	3			-	
	Skirt/Brim Minimum Length	mm	250				
Environmental Condition	Room Temperature	°C	23±2				
	Relative Humidity	% RH	50±10				

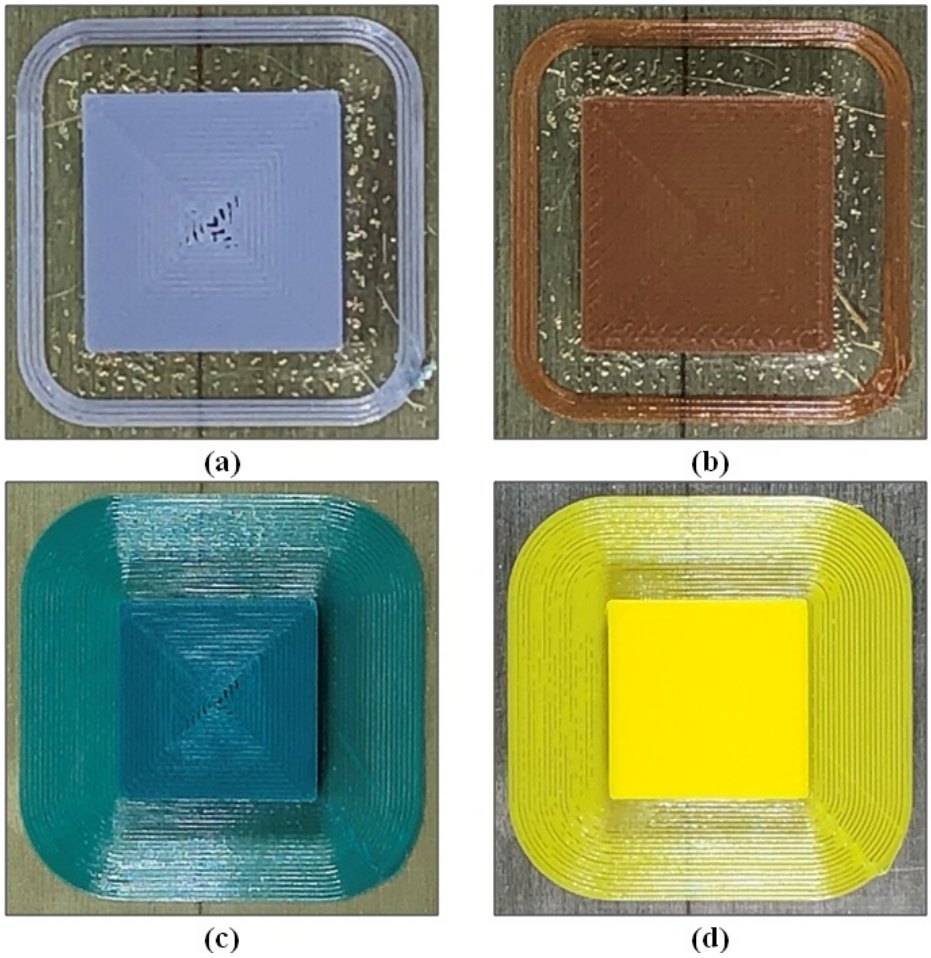

Figure 5. Fabricated model of PLA Plus (a) skirt without top/bottom thickness, (b) skirt with top/bottom thickness, (c) brim without top/bottom thickness and (d) brim with a top/bottom thickness

2.5. FDB 3D Sample Fabrication

Several samples were manufactured with independent process parameters in order to compare geometry variation, surface roughness and density. In the current study, a total of 100 "small blocks" printed parts were printed and tested (as printed size: 15 × 15 × 5 mm3 in length, width and height, respectively). Group A (from 1 to 25 samples) which belong to "skirt without top/bottom thickness". Group B (from 26 to 50 samples) which belongs to "skirt with top/bottom thickness". Group C (from 51 to 75 samples) which belongs to "brim without top/bottom thickness". Group D (from 76 to 100 samples) which belongs to "brim with top/bottom thickness". Each group has five independent printing temperatures 205°C, 210°C, 215°C, 220°C and 225°C and five independent printing speeds 30 mm/s,60 mm/s, 90 mm/s, 120 mm/s and 150 mm/s. The dimensions of the proposed sample are 15 mm × 15 mm × 5 mm in length, width and height, respectively. Figure 5 shows the sample details of printed parts for each group A, B, C and D with a processing printing time of 35 minutes (minimum) and 50 minutes (maximum). The overall printing time is highly dependent on many process parameters. Two vital manufacturing process parameters are the nozzle diameter and the inll density.

The printing samples were done on the top of the build platform surface (250 mm × 210 mm) which has as heating bed underneath (I3 MK3 model) with a laboratory 1 Ω embedded standard resistor. Once the electric current flows through each resistor in turn, due to the Joule heating effect (Joule's first law), the energy dissipated too quickly as heat to the build platform surface. Besides, the heating bed can reach 180°C with the help of the power supply.

3. Results and Discussions

There are a great many variables that can be used to evaluate the printed part quality finish. In this research, only three parameters are preliminarily evaluated. These are geometry variation (length, width and height), surface roughness profile (Ra, Rq, Rsk, Rku and Rq/Ra) and density (weight and volume). After printing using the Original Prusa I3 MK3 model, the test specimens are conditioned at normal room temperature, T, of 23±2°C and relative humidity, RH, of 50±10%, and then measured directly using the digital Vernier gauge after having been removed from the build platform surface for over one month. Each dimension was measured at least three times at a different location approximately 15 min, and the average (mean) value was considered. The standard deviation (±SD) for each dimension of the printed parts in a direction was calculated and presented as mean and standard deviation (mean±SD). The relative error, ε, and overall relative error were also calculated. The investigation explanations are discussed in detail in the following sub-section. Bear in mind that all printed parts taken in this pilot have some degree of warping deformation.

3.1. Geometry Variation Inspection

First, the influence of the printing temperature, *T*, and printing speed, *v*, on a total of 100 printed parts geometry is studied. Printing temperature, *T*, is wide-ranging from 205°C to 225°C with a 5°C increment. Printing speed, *v*, is also wide-ranging from 30 mm/s to 150 mm/s with a 30 mm/s increment. The relative error, ε, was used to evaluate the accuracy of the geometry. Here, ε is defined as follows:

$$\varepsilon = \frac{1}{3}\sum_{i=1}^{3}\varepsilon_i \quad (1)$$

$$\varepsilon_L = \frac{|l_m - l_t|}{\varepsilon_t} \quad (2)$$

$$\varepsilon_W = \frac{|l_m - l_t|}{\varepsilon_t} \quad (3)$$

$$\varepsilon_H = \frac{|l_m - l_t|}{l_t} \quad (4)$$

where ε_L, ε_W and ε_H are the relative error of length, width and height, respectively, l_m and l_t are the measured and true values of the printed parts.

Figure 6, Figure 7, Figure 8 and Figure 9 showed the length (red line) versus width (green line) variation including true (black line) and measured (red and green lines) values of group A, B, C and D along with skirt/brim with/without top/bottom thickness. It shows that there is no consistency in the dimensional deviation between the length and width of the printed parts (as stated in the true value of 15 mm × 15 mm) due to the lack of homogeneity density arising from the discontinuities in an inner filling of the small block. Figure 10 shows the polar diagram of the height variation including true and measured values. Again, over different printing temperature and speed, there is no consistency in the dimensional deviation in the height of the printed parts (as stated in the true value of 5 mm), due to the deposited material filament changes from the theoretical cylindrical shape, as it is considered an ideal cylindrical shape. Most notably, all 100 FDM 3D printed parts were set at 40 µm (layer thickness) and 100% (infill density), which requires a considerable length of time to cure for the crystallization of each layer of printed part material. So, the deviation from the ideal dimension caused by the volumetric shrinkage/enlargement is quite visible. Generally, the large deviation happens due to the rough temperature difference of the deposited material (205°C, 210°C, 215°C, 220°C and 225°C), the deposition platform (60°C) and the environmental temperature (23°C). Moreover, as the temperature increased, the geometry deviation increased as well and likewise with the printing speed indicating that more filament material will be deposited on the build platform surface and more vibration will affect the metrology loop of the FDM 3D printer.

In group A, as shown in Figure 6 and Figure 10(a), the maximum deviation size of the printed parts (1 - 25) at independent printing temperatures and independent printing speed was increased to 15.07×15.16×5.10 mm^3 after printing, showing 0.47%, 1.05% and 1.96% enlarged in length, width and height, respectively. This indicates a volumetric enlargement of 3.48% compared to the original STL file. The minimum deviation size of the printed parts was reduced to 14.96×14.98×4.98 mm^3 after printing, showing 0.27%, 0.13% and 0.4% shrinkage in length, width and height, respectively. This indicates a volumetric shrinkage of 0.8% compared to the original STL file. The total maximum deviation (±SD) was ±0.04 mm in length and height while ±0.07 mm in width with a minimum deviation of ±0.01 mm in length, width and height.

In group B, as shown in Figure 7 and Figure 10(b), the maximum deviation size of the printed parts (26 - 50) at independent printing temperatures and independent printing speeds were increased to 15.01×15.04×5.10 mm^3 after printing, showing 0.067%, 0.266% and 1.961% enlargements in length, width and height, respectively. This indicates a volumetric enlargement of 2.29% compared to the original STL file. The minimum deviation size of the printed parts was reduced to 14.76×14.94×4.99 mm^3 after printing, showing 1.60%, 0.4% and 0.2% shrinkage in length, width and height, respectively. This indicates a volumetric shrinkage of 2.2% compared to the original STL file. The total maximum deviation (±SD) was ±0.09 mm in length and ±0.04 mm in width and height with a minimum deviation of ±0.01 mm in length, width and height.

In group C, as shown in Figure 8 and Figure 10(c), the maximum deviation size of the printed parts (51 - 75) at independent printing temperatures and independent printing speeds was increased to 15.18×15.24×5.16 mm^3 after printing, showing 1.185%, 1.574% and 3.1% enlargements in length, width and height, respectively. This indicates a volumetric enlargement of 5.859% compared to the original STL file. The minimum deviation size of the printed parts was reduced to 14.97×14.96×4.99 mm^3 after printing, showing 0.2%, 0.27% and 0.2% shrinkage in length, width and height, respectively. This indicates a volumetric shrinkage of 0.67% compared to the original STL file. The total maximum deviation (±SD) was ±0.09 mm, ±0.11 and ±0.05 in length, width and height, respectively, with a minimum deviation of ±0.01 mm in length, width and height.

In group D, as shown in Figure 9 and Figure 10(d), the maximum deviation size of the printed parts (76 - 100) at independent printing temperatures and independent printing speeds was increased to 15.09×15.12×5.06 mm^3 after printing, showing 0.596%, 0.795% and 1.185% enlargements in length, width and height, respectively. This indicates a volumetric enlargement of 2.579% compared to the original STL file. The minimum deviation size of the printed parts was reduced to 14.98×14.98×4.98 mm^3 after printing, showing 0.13%, 0.13% and 0.4% shrinkage in length, width and height, respectively. This indicates a volumetric shrinkage of 0.66% compared to the original STL file. The total maximum deviation (±SD) was ±0.05 mm in length, width and height, respectively, with a minimum deviation of ±0.02 mm in length and ±0.01 width and height.

It can be concluded that for length, width and height variation, group C (brim without top/bottom thickness) represent the highest deviation from the true value by almost ~5.859% and group B (skirt without top/bottom

thickness) represent the lowest deviation from the true value by almost ~2.29%. Even if the printing process parameter of the layer height was set at 40 µm, which in fact will minimize the total layer printing and cost-effectiveness, the initial printed layer/path (first layer/path) was cooled just before the deposition of the following layer/path, resulting in a weak bonding and high porosity between rasters and layers. This is conceivably due to the high melt flow rate under FDM 3D printing conditions, which is reflected by the lower viscosity of molten material properties that are associated with higher polymerization shrinkage. The total deviation is an acceptable range of tolerance as overall of each piece of RP.

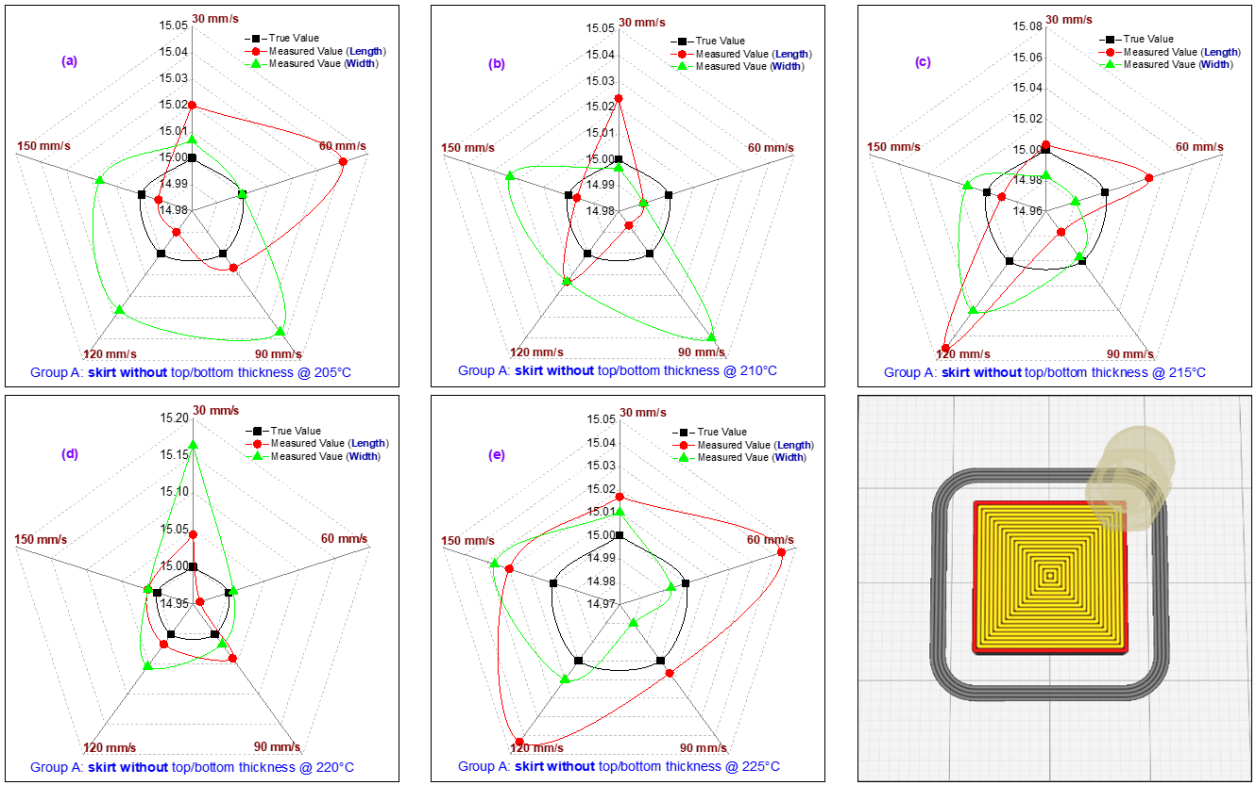

Figure 6. Length versus width variation including true and measured values of group A (skirt without top/bottom thickness)

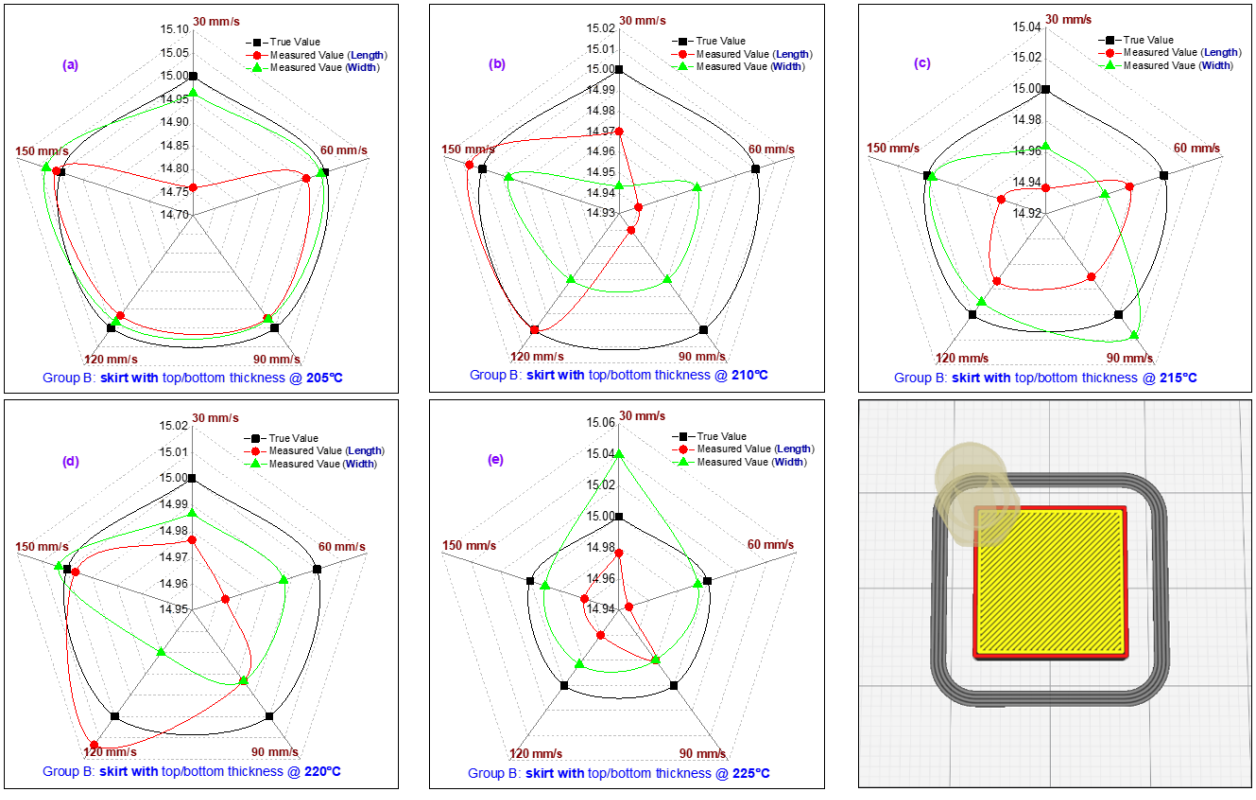

Figure 7. Length versus width variation including true and measured values of group B (skirt with top/bottom thickness)

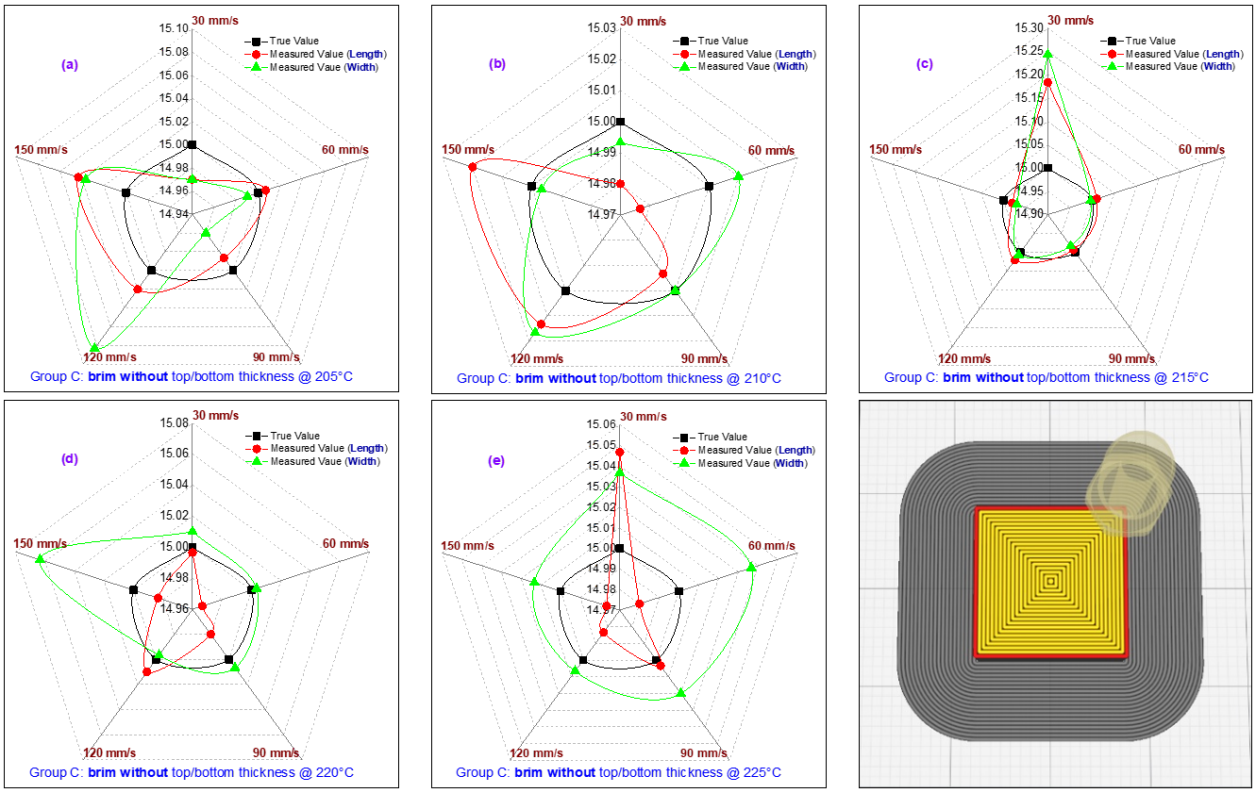

Figure 8. Length versus width variation including true and measured values of group C (brim without top/bottom thickness)

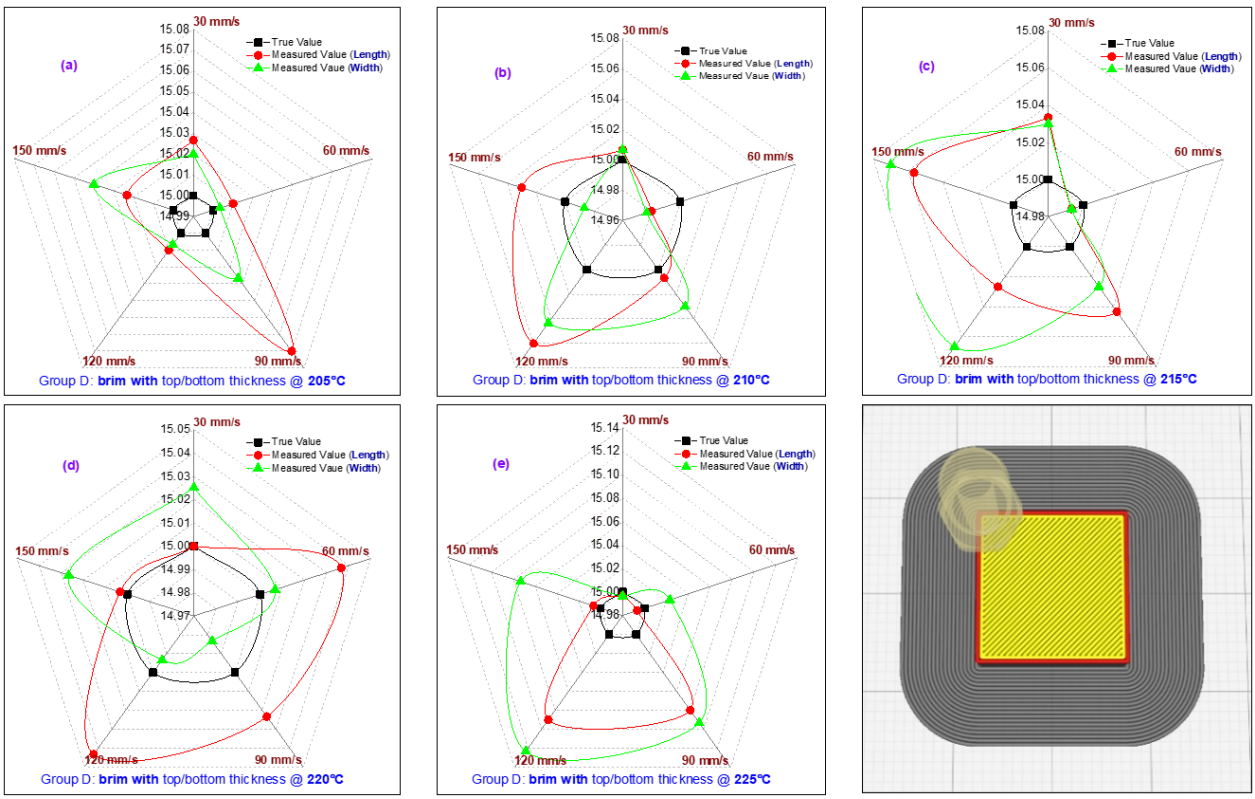

Figure 9. Length versus width variation including true and measured values of group D (brim with a top/bottom thickness)

The relative errors, ε, were calculated and plotted in Figure 11. Bear in mind, the printing temperature, *T*, is varied from 205°C to 225°C with a 5°C increment. Also, the printing speed, *v*, is also varied from 30 mm/s to 150 mm/s with a 30 mm/s increment. The total mean value and standard deviation (mean±SD) of the relative error, ε, for 100 FDM 3D printed samples was 0.9079±0.3809%, 0.9028±0.3733%, 1.0521±0.5163% and 0.9809±0.4982% in group A, B, C and D respectively. The total accuracy of the relative error was 99.09%, 99.09%, 98.95% and 99.02% in group A, B, C and D respectively. Group C (brim without top/bottom thickness) represents the highest relative error while group B skirt with top/bottom thickness represents the lowest relative error. Thus is, the

relative error, ε, of group C > relative error of group D > relative error of group A > relative error of group B. Noticed that the relative error, ε, of group A and group B was in very close proximity to each other with a minor difference of 0.0051% (99.99% accuracy) and group C and group D was in very close proximity to each other with a minor difference of 0.0712% (99.92% accuracy).

In group A, the mean and standard deviation (mean±SD) of relative error, ε, was 0.1511±0.1124%, 0.1591±0.2126% and 2.4133±0.3809% in length, width and height, respectively, with maximum and minimum value of 0.4667% and 0.0222% in length, 1.0889% and 0.0001% in width and 3.8000% and 1.3333% in height, respectively. In group B, the mean and standard deviation (mean±SD) of relative error, ε, was 0.2587±0.3033%, 0.1484±0.0900% and 2.3013±0.7268% in length, width and height, respectively, with maximum and minimum value of 1.6000% and 0.0001% in length, 0.3778% and 0.0222% in width and 3.2667% and 0.9333% in height, respectively. In group C, the mean and standard deviation (mean±SD) of relative error, ε, was 0.1680±0.2316%, 0.1964±0.3265% and 2.7920±0.9909% in length, width and height, respectively, with a maximum and minimum value of 1.2222% and 0.0222% in length, 1.6222% and 0.0001% in width and 5.0000% and 0.9333% in height, respectively. In group D, the mean and standard deviation (mean±SD) of relative error, ε, was 0.1929±0.1708%, 0.2164±0.2042% and 2.5333±1.1195% in length, width and height, respectively, with a maximum and minimum value of 0.6000% and 0.0001% in length, 0.8222% and 0.0222% in width and 6.2667% and 0.9333% in height, respectively. The standard deviation in all groups was too high due to independent printing process parameters during the 100 FDM 3D printed parts.

This shows that the relative error, ε, increased by increasing the printing temperature due to the liquidity of the PLA Plus increase and that the geometrical accuracy of the printed parts geometrical becomes hard to control with the high liquidity of the thermoplastic filament materials. At 205°C printing temperature, the relative error, ε, increased as the printing temperatures decreased. That might be true, and it might be explained by the fact that the PLA Plus thermoplastic filament material is not fully molten during processing and is therefore hard to squeeze out below its melting point of temperature. Therefore, high or even very high friction (tribological effect) during the extrusion process from the nozzle affects the geometrical accuracy resulting in a large relative error.

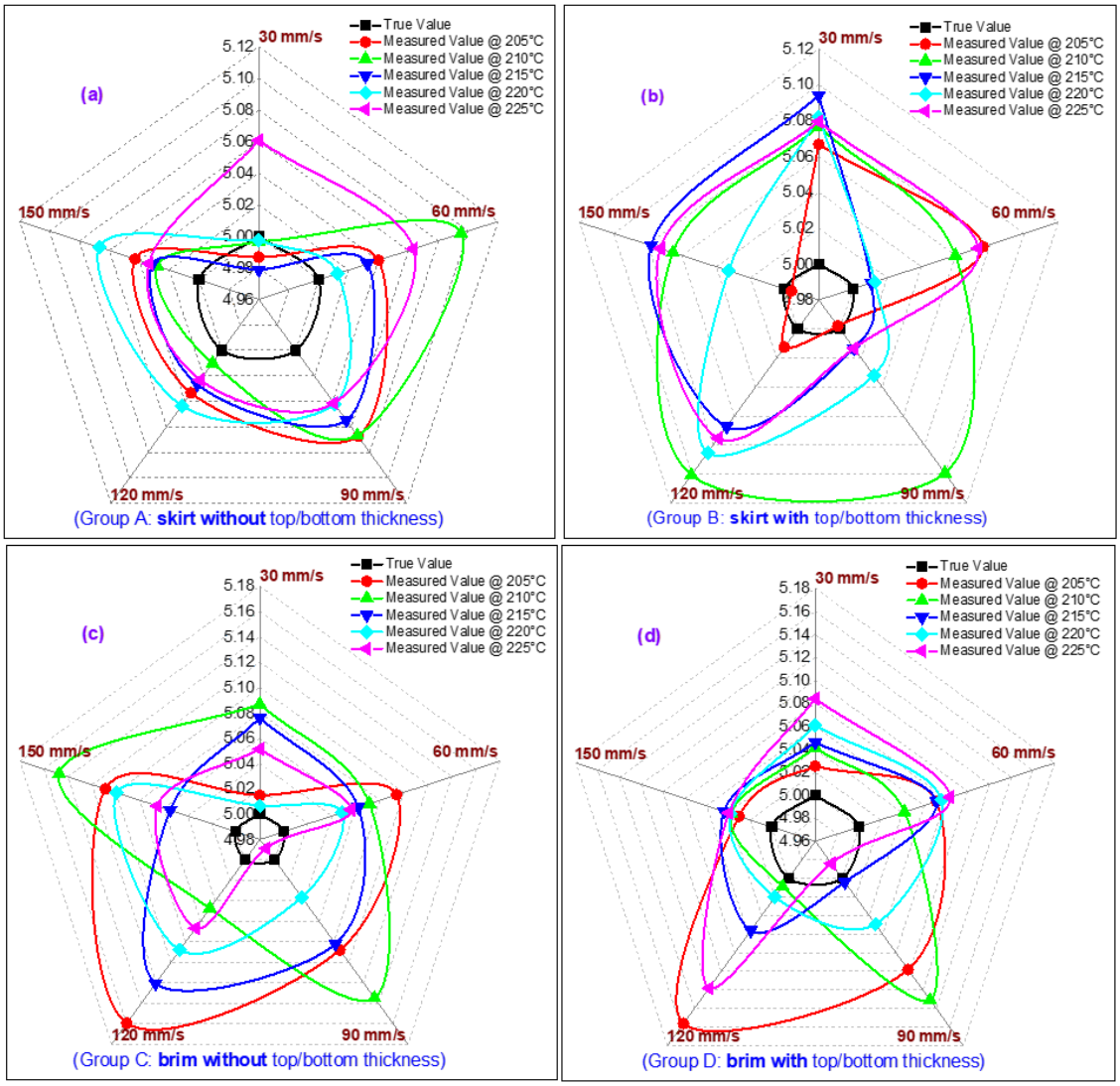

Figure 10. Height variation including true and measured values (a) skirt without top/bottom thickness, (b) skirt with top/bottom thickness, (c) brim without top/bottom thickness and (d) brim with a top/bottom thickness

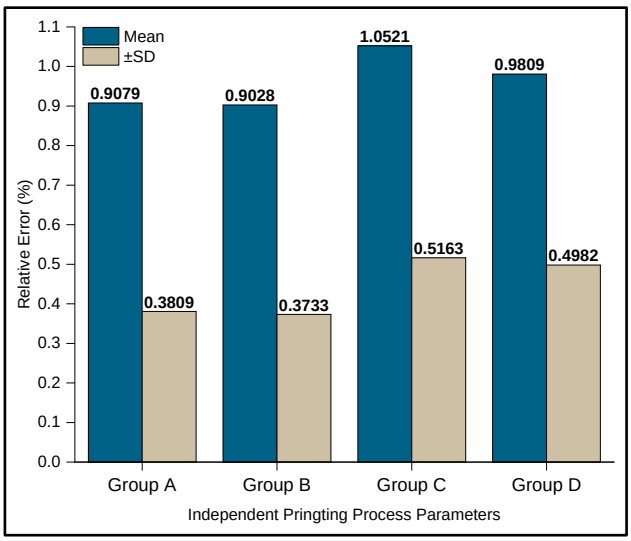

Figure 11. Relative error of (group A: skirt without top/bottom thickness), (group B: skirt with top/bottom thickness), (group C: brim without top/bottom thickness and (group D: brim with a top/bottom thickness)

It also can be predicted that the relative error, ε, would be higher than the relative error, ε, below 205°C even if the fabrication process is accomplished due to micro- and nano-tribology issues. The printing temperature at 220°C is appropriate and recommended in this study. The relative error, ε, of the FDM 3D printed part is noticeably large when the printing speed is too fast or even too slow as well as due to extrusion heat being focused on the printed part and heat dissipation being relatively poor. High printing speed also leads to vibration of the FDM 3D printer (the rigid body or metrology loop) leading to an increase in the relative error.

3.2. Surface Roughness Profile Inspection

Second, the influence of the printing temperature, *T*, and printing speed, *v*, on the surface roughness profile (R_a, R_{sk}, R_{ku} and R_q/R_a) is studied. Printing temperature, *T*, is wide-ranging from 205°C to 225°C with a 5°C increment. Printing speed, *v*, is also wide-ranging from 30 mm/s to 150 mm/s with a 30 mm/s increment. Figure 12 shows the specimen holder with a located specimen is correctly positioned within a precision machine.

In surface roughness profile inspection, with a best combination of almost 0.7 mN low contact force, 50 nm high sensitivity displacement and a small stainless steel tip radius of a 2 µm stylus being used on FDM 3D printed parts, the distribution of surface roughness potential irregularities of the 100% infill density FDM 3D printed parts was assessed by a conventional contact-type Taly-Surf® surface roughness profilometer from Taylor Hobson Precision, Inc. The inspections were completed under the fundamental friction and wear-free perception and high-precision and high-accuracy measurement, which provided high spatial resolution down to 0.8 nm, a measuring instrument range (*x*-axis) of 12.5 mm, and linear mode speed up to 0.5 mm/s or higher. The traces were auto-leveled direction and set-up to a linear least-squares (LLS) fitting technique (single scan mode) and after that is filtered with a standard low-pass filter (LPF) of 0.8 mm effective cut-off wavelength. Full details of the measurement procedure have been reported elsewhere [18-22]. The calibration results using a standard ball of 22.0161 mm diameter (from Taylor Hobson Precision, Ltd.) after a series of trials showed that the system of the one-end cantilever beam was a linear mass-spring system regression of $R^2 > 0.99$, under various working and eco-friendly issues, with an absolute value of each uncertainty of <1% and displacement measurement resolution down to at worst performance of 50 nm.

The measurements were conducted in two directions of 15 mm (length) × 15 mm (width). The assessment was conducted at least three times and the average of three measured values was taken as R_a, R_q, R_{sk}, R_{ku} and R_q/R_a for each measurement. The Surface roughness profile of each FDM 3D printed part is calculated by

$$R_a = \frac{R_{a(length)} + R_{a(width)}}{2} \quad (5)$$

$$R_q = \frac{R_{q(length)} + R_{q(width)}}{2} \quad (6)$$

$$R_{sk} = \frac{R_{sk(length)} + R_{sk(width)}}{2} \quad (7)$$

$$R_{ku} = \frac{R_{ku(length)} + R_{ku(width)}}{2}. \quad (8)$$

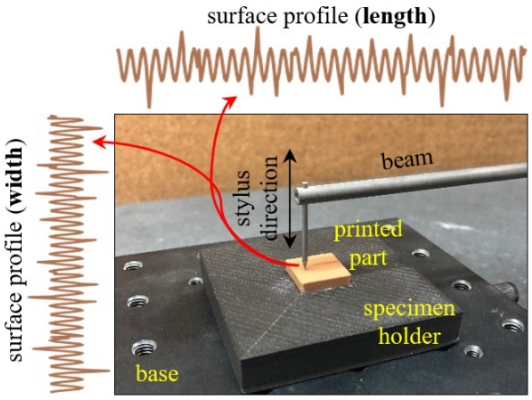

Figure 12. Image of Taly-surf® with conisphere tip r = 2 µm (from Taylor Hobson) and specimen holder with a located specimen correctly positioned within a precision machine

Figure 13 shows the significantly different condition in the surface roughness height profile behaviour of length and width along "with" and "without" top/bottom thickness after fabricated using PLA Plus thermoplastic filament material. It shows the frequent wider peaks-to-valleys distribution indicating that the printing process parameters controlled the surface quality finish. The fabricated part follows the top direction pattern of the STL file. The obtained data generated from Figure 13 (a) show that the behaviour of the surface roughness distribution region of the FDM 3D printed parts without top/bottom thickness is rough, -119.163 µm < surface profile < +22.403 µm with ±15.6297 µm deviation in length and -89.844 µm < surface profile < +32.895 µm with ±12.4137 µm deviation in width. However, the obtained data generated from Figure 13 (b) show that the behaviour of the surface roughness distribution region of the FDM 3D printed parts with top/bottom thickness is smooth, -4.04 µm < surface

profile < +6.692 µm with ±2.19 µm deviation in length and -3.569 µm < surface profile < +2.913 µm with ±1.9801 µm deviation in width.

Surprisingly, the R_a of printed parts "with" and "without" top/bottom thickness, as shown in Figure 13, was almost the same and consistency for both axes (length and width) with a small difference of ~10% in each axis. In the case of "without top/bottom thickness", the average surface roughness was 7.5793 µm and 6.8997 µm, respectively. In the case of "with tip/bottom thickness" the average surface roughness was 1.7930 µm and 1.6082 µm, respectively. This behaviour of the surface roughness is indicating that the surface roughness improved by almost by ~80% in both axes when using top/bottom thickness compared to the concentric pattern.

In Figure 13(a), the surface roughness profile parameter ratio performance, R_q/R_a, (root means square, R_q, to average surface roughness, R_a) did not follow the similar periodic trend of the surface texture across the 10 mm assessment of about ~2.06 and ~1.80 in length and width, respectively. While in Figure 13(b), the surface roughness profile parameter ratio performance, R_q/R_a, (root means square roughness, R_q, to arithmetic average surface roughness, R_a) has a tendency in general to follow the same periodic trend of the surface texture across the 10 mm assessment of about ~1.22 and ~1.23 in length and width, respectively.

Figure 14 shows the surface roughness performance of the 100 FDM 3D printed samples versus independent printing speeds (30, 60, 90, 120, 150 mm/s) and independent printing temperatures (205, 210, 215, 220, 225°C). In general, at 30 mm/s printing speed and 215°C printing temperature, the R_a represents the highest surface roughness by reaching 17.19 µm, which is desirable for biomaterial applications, while at 150 mm/s printing speed and 220°C printing temperature, the R_a represents the lowest surface roughness by reaching 1.08 µm, indicating that the reduction improved by almost ~94%. What is more, variations were noticed in the surface roughness, R_a, distribution curves and are caused by the differences between the schematic 3D digital file (STL file) and the real surface profile, quite a lot of micro-sized burrs and irregular steps. This fact leads to each surface roughness distribution of 100 FDM 3D printed parts having its own characteristics.

Figure 14(a) represents the surface roughness of the 25 samples (group A: skirt without top/bottom thickness). The maximum and minimum R_a over independent printing speed, v, and temperature, T, were 17.19 µm and 2.48 µm, respectively, with the total mean and standard deviation value of 5.6820±3.6804 µm. Generally, 30 mm/s shows high R_a despite the low nozzle (0.4 mm) diameter, suggesting a minor effect of the 0.4 mm nozzle diameter on the surface roughness profile (amplitude), while other independent printing process parameters such as printing speed, v, showed low and fluctuated R_a over independent printing temperature.

Figure 14(b) represents the surface roughness of the 25 samples (group B: skirt with top/bottom thickness). The maximum and minimum R_a over independent printing speed, v, and temperature, T, were 4.71 µm and 1.45 µm, respectively, with the total mean and standard deviation value of 2.1312±0.9085 µm. Generally, the R_a fluctuated over the printing temperature. Unlike Figure 14(a), the printed parts surface finish with top/bottom thickness was improved by almost ~73% and ~42% for the maximum and minimum R_a, respectively.

Figure 14(c) represents the surface roughness of the 25 samples (group C: brim without top/bottom thickness). The maximum and minimum R_a over independent printing speed, v, and temperature, T, were 16.41 µm and 2.72 µm, respectively, with the total mean and standard deviation value of 5.4842±2.8048 µm. Generally, the R_a fluctuated over the independent printing temperature.

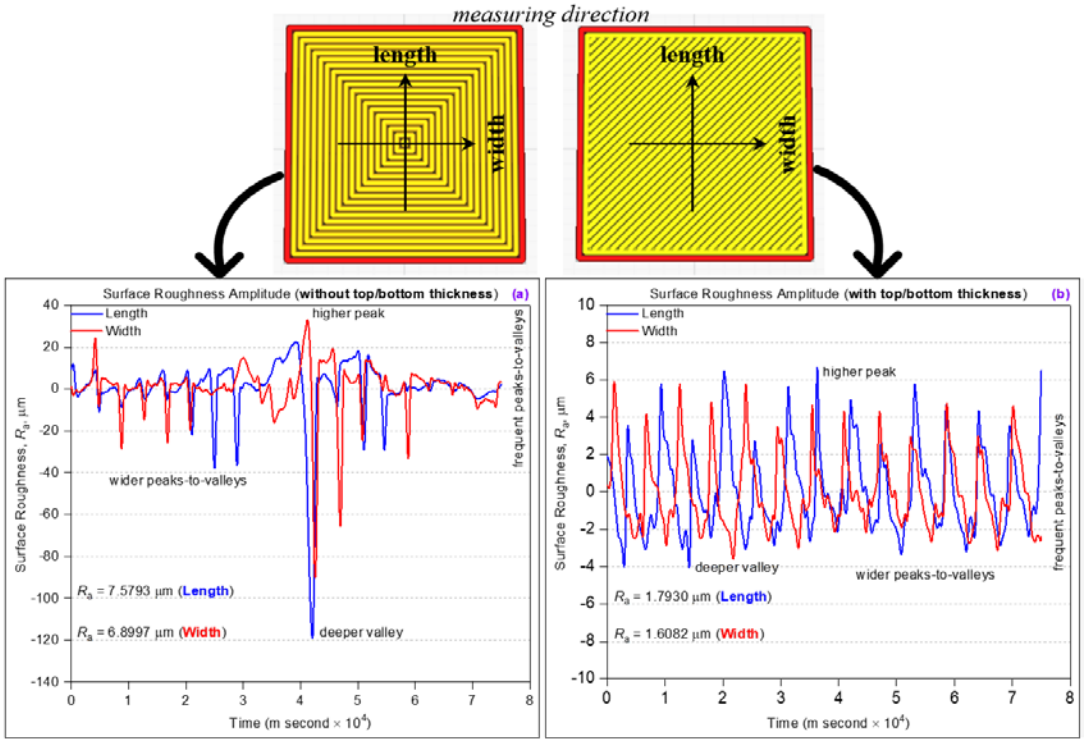

Figure 13. Surface roughness height profile of length and width (a) without top/bottom thickness and (b) with a top/bottom thickness

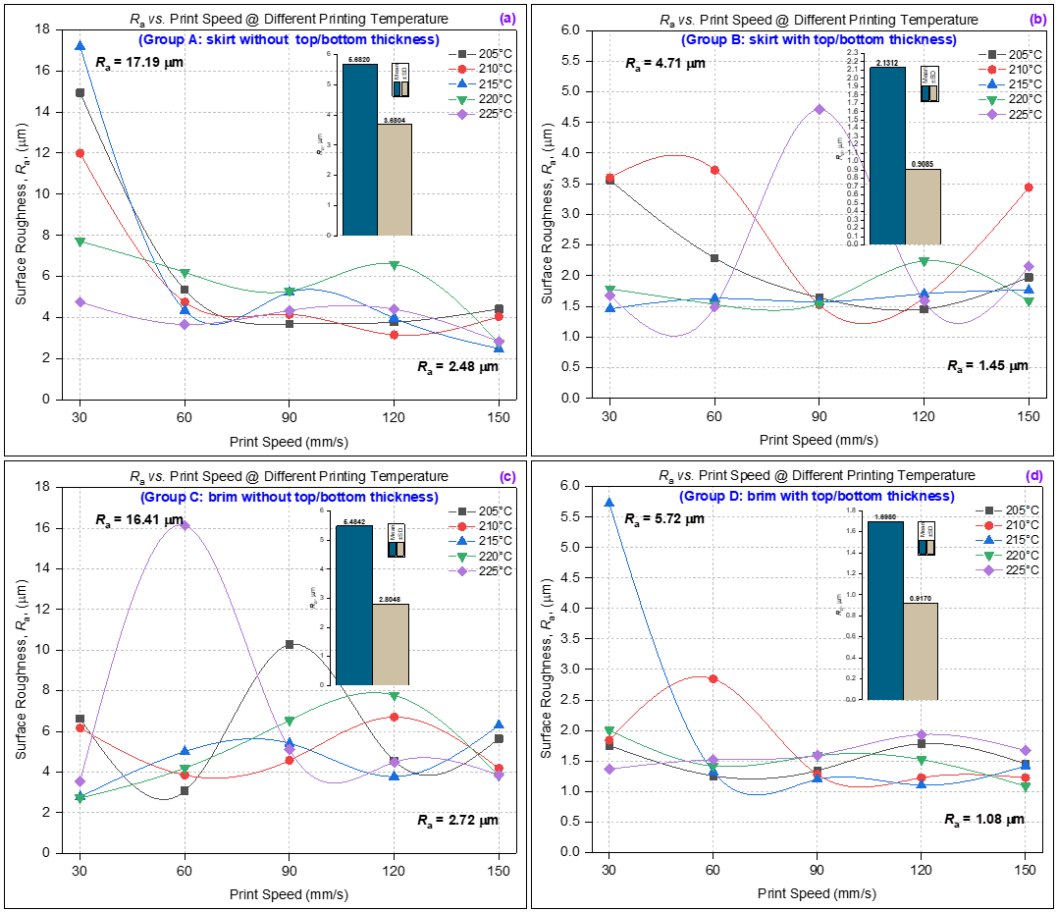

Figure 14. Surface roughness versus print speed @ different printing temperature (a) skirt without top/bottom thickness, (b) skirt with top/bottom thickness, (c) brim without top/bottom thickness and (d) brim with a top/bottom thickness

Figure 14(d) represents the surface roughness of the 25 samples (group D: brim with top/bottom thickness). The maximum and minimum R_a over independent printing speed, v, and temperature, T, were 5.72 µm and 1.08 µm, respectively, with the total mean and standard deviation value of 1.6980±0.9170 µm. Generally, the R_a fluctuated over the independent printing temperature. Unlike Figure 14(c), the FDM 3D printed parts surface finish with top/bottom thickness was improved by almost ~65% and ~60% for the maximum and minimum R_a, respectively.

In general, the differences in the surface roughness, R_a, of the FDM 3D printed parts were significant. The surface roughness of FDM 3D printed parts was influenced by "with top/bottom thickness" (skirt or brim) more than "without top/bottom thickness" (skirt or brim) at 40 µm layer height. These results are apparent as the skirt/brim with top/bottom thickness will follow different infill directions as the top and bottom layer deposited using 45° orientation build while skirt/brim without top/bottom thickness will follow the concentric pattern as the infill density. Low surface roughness was achieved by almost 1.08 µm and high surface roughness was also achieved by almost 17.19 µm. These data surfaces roughness depend on the machine repeatability and precision. Therefore, these are the key factors to be taken into consideration. High surface roughness, R_a, is required for bio-materials applications because it is associated with cell proliferation and cell attachment of bone resulting in an implant stability improvement.

Figure 15(a) shows the R_q/R_a ratio performance of group A (1 - 25). It is worth mentioning that the ratio performance, R_q/R_a, is an average value of group A of the first 25 FDM 3D printed parts. Particularly satisfactory is that the R_q/R_a ratio is almost equivalent to an empirical value of ~1.22 (for a 2D geometric model) with a slight deviation which is an admirable surface profile ratio, as the R_q parameter is much more sensitive to irregular high peaks and deep valleys of the assessed roughness profile than the R_a parameter because of the fact that the amplitudes of R_q are squared. Geometrically, the maximum ratio, R_q/R_a, of root means square, R_q, to average surface roughness, R_a, was found to be ~2.76 while the minimum ratio, R_q/R_a, of root means square, R_q, to average surface roughness, R_a, was found to be ~1.23 with a total standard deviation (±SD) of ±0.45 and the mean value of the 25 printed parts observations was found to be ~1.57, indicating that the ratio is some distance from the empirical value by almost 22.3%.

Figure 15(b) shows the R_q/R_a ratio performance of group B (26 - 50). Worth mentioning that the ratio performance, R_q/R_a, is an average value of group B of the second 25 FDM 3D printed parts. The maximum ratio, R_q/R_a, of root means square, R_q, to average surface roughness, R_a, was found to be ~1.77 while the minimum ratio, R_q/R_a, of root means square, R_q, to average surface roughness, R_a, was found to be ~1.18 with a total standard deviation (±SD) of ±0.19 and the mean value of the 25 printed parts observations was found to be ~1.36, indicating that the ratio is some distance from the empirical value by almost 10.3%.

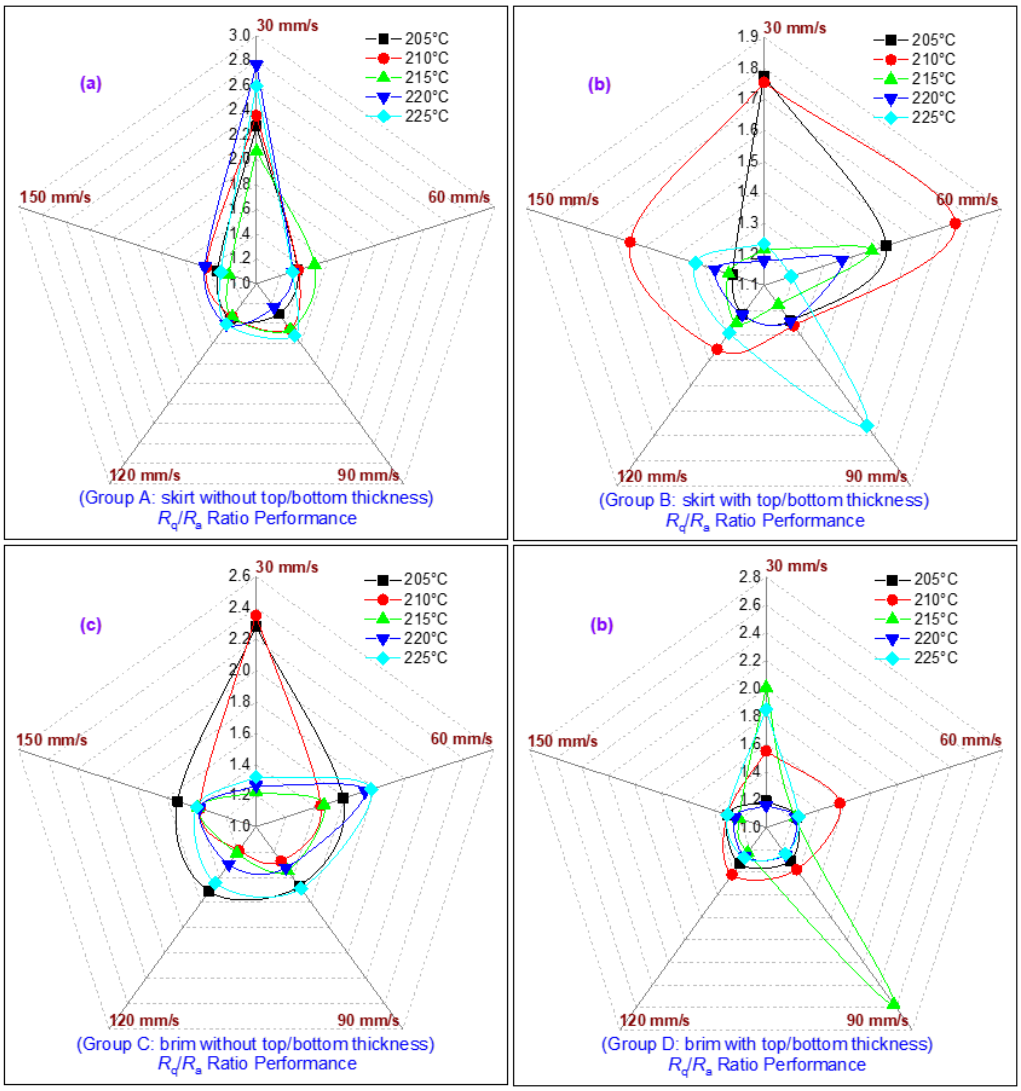

Figure 15. Surface profile (2D) of R_q/R_a (a) skirt without top/bottom thickness, (b) skirt with top/bottom thickness, (c) brim without top/bottom thickness and (d) brim with a top/bottom thickness

Figure 15(c) shows the R_q/R_a ratio performance of group C (51 - 75). It is worth mentioning that the ratio performance, R_q/R_a, is an average value of group C of the third 25 FDM 3D printed parts. The maximum ratio, R_q/R_a, of root means square, R_q, to average surface roughness, R_a, was found to be ~2.35 while the minimum ratio, R_q/R_a, of root means square, R_q, to average surface roughness, R_a, was found to be ~1.19 with a total standard deviation (±SD) of ±0.29 and the mean value of the 25 printed parts observations was found to be ~1.48, indicating that the ratio is some distance from the empirical value by almost 17.6%.

Figure 15(d) shows the R_q/R_a ratio performance of group D (76 - 100). It is worth mentioning that the ratio performance, R_q/R_a, is an average value of group D of the fourth 25 FDM 3D printed parts. The maximum ratio, R_q/R_a, of root means square, R_q, to average surface roughness, R_a, was found to be ~2.57 while the minimum ratio, R_q/R_a, of root means square, R_q, to average surface roughness, R_a, was found to be ~1.16 with a total standard deviation (±SD) of ±0.32 and the mean value of the 25 printed parts observations was found to be ~1.39, indicating that the ratio is some distance from the empirical value by almost 12.2%.

The third-order central moment (measure for the degree of symmetry, positive or negative, in the variable distribution) and fourth-order central moment (measure for the degree of peakedness/flatness, tall or flat, in the variable distribution) are skewness, R_{sk}, (3^{rd} central moment) and kurtosis, R_{ku}, (4^{th} central moment), respectively, which both provide very useful data on the real surface distribution profile of FDM 3D printed part, which is also both (skewness, R_{sk}, and kurtosis, R_{ku},) going to be discussed here in more detail.

Skewness, R_{sk}, as shown in Figure 16(a), is well-defined by ISO 4287 (1997) [37] as it evaluates the degree of asymmetry distribution and is categorized as positively skewed distribution, $R_{sk} > 0$, (surfaces are 'empty' of material) or negatively skewed distribution, $R_{sk} < 0$, (printed parts' surface profile is "full" of filament material). It is a very important parameter for micro- and nano-tribological applications involving as it does friction, wear and lubrication. Normal distribution (Gaussian distribution) presents $R_{sk} = 0$ (symmetrical). Kurtosis, R_{ku}, as shown in Figure 16(b), is well-defined by ISO 4287 (1997) [37] as it evaluates the distribution sharpness with $R_{ku} = 3$ (mesokurtic distribution) for the normal distribution. The surface profile is influenced by sharp

peaks (spiky) surface when R_{ku} > 3 (leptokurtic distribution with high degree of peakedness), while the surface profile is influenced by bumpy peaks surface when R_{ku} < 3 (platykurtic distribution with low degree of peakedness). In this regard, R_{ku} is very important assessment parameter as regards providing very useful information on the real contact area of thermoplastic filament material and friction/wear resistance. Also, it is more likely to distinguish the periodicity of the surface profile assessment (R_{ku} < 3).

Figure 17 demonstrates the skewness, R_{sk}, (3rd central moment) versus the kurtosis, R_{ku}, (4th central moment) of 100 FDM 3D printed parts. Preferably, a value of zero for skewness, R_{sk}, and three for kurtosis, R_{ku}, is characteristic for a weakly isotropic Gaussian random.

In Figure 17(a), the general tendency of a data series of PLA Plus thermoplastic filament material (group A: skirt without top/bottom thickness) showed positively skewed distribution (+R_{sk} for steep peaks and flat valleys) and negatively skewed distribution (-R_{sk} for flat peaks and steep valleys) but then was not distributed equally between ±R_{sk}, which is more likely to be (-R_{sk}) negatively skewed distribution by almost ~80% rather than (+R_{sk}) positively skewed distribution by almost ~20% for surface profile. Also, it showed both leptokurtic (fat-tailed) and platykurtic (thin-tailed) distribution with high and low degree of peakedness, as R_{ku} registered both fewer and greater than 3. The maximum and minimum approximate trend of skewness, R_{sk}, and kurtosis, R_{ku}, as numerical measures of the shape of data was in the range of $-7.09 \leq R_{sk} \leq 0.74$ and $2.52 \leq R_{ku} \leq 66.31$, with mean and standard deviation (mean±SD) of -1.52±1.94 and 10.74±13.00, respectively. Besides, the maximum range was 7.83 and 63.79 for R_{sk} and R_{ku}, respectively.

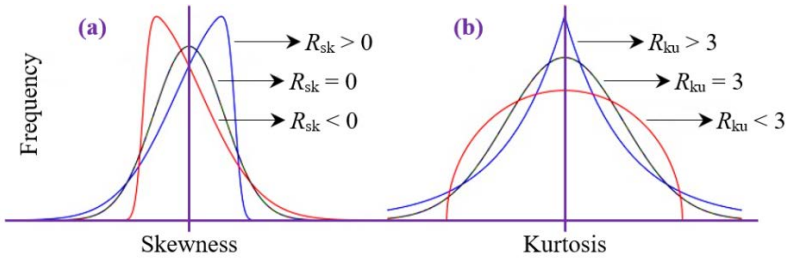

Figure 16. Skewness versus kurtosis distribution

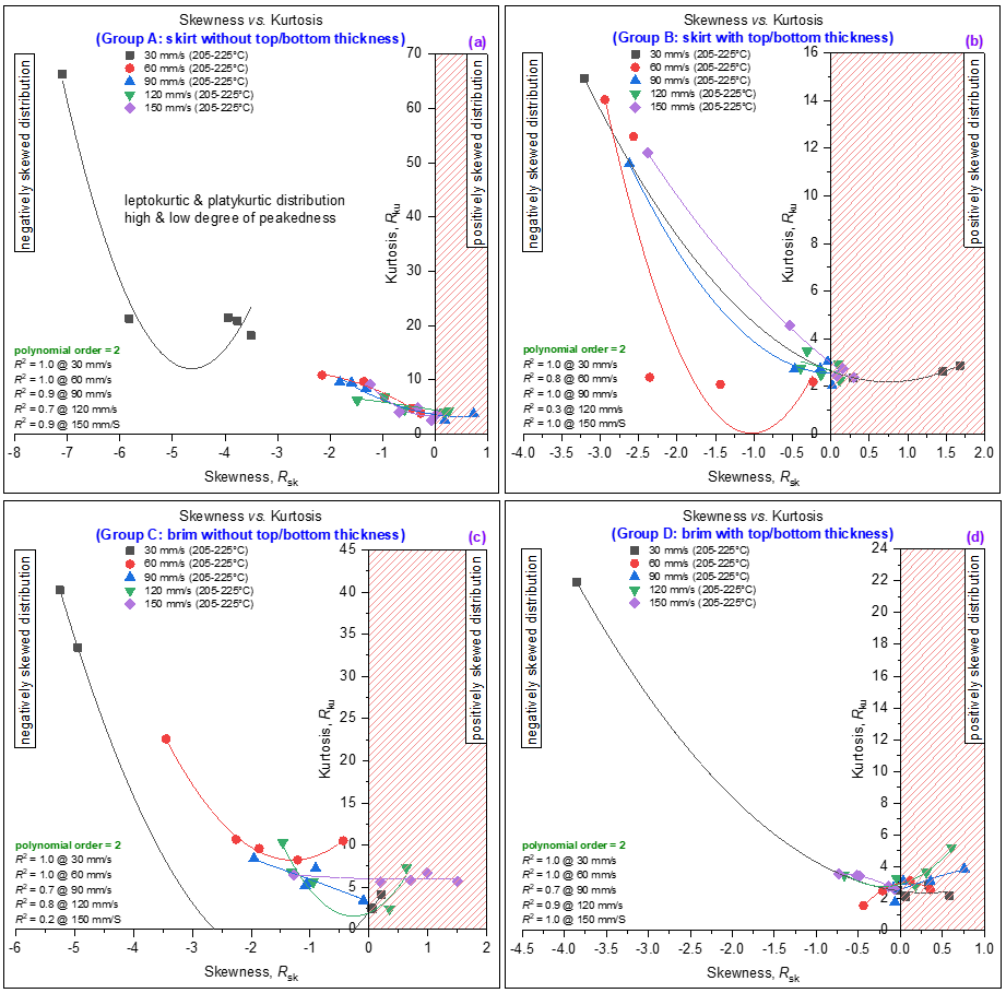

Figure 17. Skewness versus kurtosis (a) skirt without top/bottom thickness, (b) skirt with top/bottom thickness, (c) brim without top/bottom thickness and (d) brim with a top/bottom thickness

In Figure 17(b), the general tendency of a data series of PLA Plus thermoplastic filament material (group B: skirt with top/bottom thickness) showed positively skewed distribution (+R_{sk} for steep peaks and flat valleys) and negatively skewed distribution (-R_{sk} for flat peaks and steep valleys) but then was not distributed equally between ±R_{sk}, which is more likely to be (-R_{sk}) negative skewed distribution by almost ~64% rather than (+R_{sk}) positively skewed distribution by almost ~36% for surface profile. Also, it showed both leptokurtic (fat-tailed) and platykurtic (thin-tailed) distribution with high and low degree of peakedness, as R_{ku} registered both fewer and greater than 3. The maximum and minimum approximate trend of skewness, R_{sk}, and kurtosis, R_{ku}, as numerical measures of the shape of data was in the range of $-3.21 \leq R_{sk} \leq 1.68$ and $2.03 \leq R_{ku} \leq 14.95$, with mean and standard deviation (mean±SD) of -0.74±1.41 and 5.23±4.69, respectively. Besides, the maximum range was 4.89 and 12.92 for R_{sk} and R_{ku}, respectively.

In Figure 17(c), the general tendency of a data series of PLA Plus thermoplastic filament material (group C: brim without top/bottom thickness) showed positively skewed distribution (+R_{sk} for steep peaks and flat valleys) and negatively skewed distribution (-R_{sk} for flat peaks and steep valleys) but then was not distributed equally between ±R_{sk}, which is more likely to be (-R_{sk}) negatively skewed distribution by almost ~64% rather than (+R_{sk}) positive skewed distribution by almost ~36% for surface profile. Also, it showed both leptokurtic (fat-tailed) and platykurtic (thin-tailed) distribution with high and low degree of peakedness, as R_{ku} registered both fewer and greater than 3. The maximum and minimum approximate trend of skewness, R_{sk}, and kurtosis, R_{ku}, as numerical measures of the shape of data was in the range of $-5.25 \leq R_{sk} \leq 1.50$ and $2.44 \leq R_{ku} \leq 40.24$, with mean and standard deviation (mean±SD) of -0.99±1.67 and 9.48±9.21, respectively. Besides, the maximum range was 6.75 and 37.8 for R_{sk} and R_{ku}, respectively.

In Figure 17(d), the general tendency of a data series of PLA Plus thermoplastic filament material (group D: brim with top/bottom thickness) showed positively skewed distribution (+R_{sk} for steep peaks and flat valleys) and negatively skewed distribution (-R_{sk} for flat peaks and steep valleys) but then was not distributed equally between ±R_{sk}, which is more likely to be (-R_{sk}) negative skewed distribution by almost ~56% rather than (+R_{sk}) positive skewed distribution by almost ~44% for surface profile. Also, it showed both leptokurtic (fat-tailed) and platykurtic (thin-tailed) distribution with high and low degree of peakedness, as R_{ku} registered both fewer and greater than 3. The maximum and minimum approximate trend of skewness, R_{sk}, and kurtosis, R_{ku}, as numerical measures of the shape of data was in the range of $-3.86 \leq R_{sk} \leq 0.76$ and $1.55 \leq R_{ku} \leq 21.94$, with mean and standard deviation (mean±SD) of -0.15±0.86 and 3.70±3.87, respectively. Besides, the maximum range was 4.62 and 20.39 for R_{sk} and R_{ku}, respectively.

3.3. Density Inspection

Third, the influence of the printing temperature, *T*, and printing speed, *v*, on the density (weight and volume) is studied. All 100 FDM 3D printed parts were built with a 100% infill density and concentric pattern so that they are manufactured with maximum material density. Such bulk density control might be used to maximize best the productivity of FDM 3D printed parts strength or reduce weight, time and cost. All the specimens were weighed with an electronic balance. The density (g/cm^3) of the thermoplastic filament material (PLA Plus) is measured merely using weight (g) divided by the volume (cm^3) of the thermoplastic filament material. Figure 18 shows the relationship between the printing speed and its corresponding filament's density concerning printing temperature. In this stage, the printing temperature, *T*, was varied from 205°C to 225°C with an increment of 5°C and the printing speed, *v*, was varied from 30 mm/s to 150 mm/s with an increment of 30 mm/s. In general, the density of the filament was slightly increased and decreased (fluctuated) over the range of printing speed and printing temperature.

The obtained data were examined using the paired-sample *t*-Test (Hypothesis Testing) at 95% of the confidence level to assess batch variations using OriginLab 2019 data analysis software. For all results, *p*-values (the probability of observed or more extreme results assuming that the null hypothesis is true (also known as α error) were determined and highly considered not significant if the obtained value is larger than 0.05 (the total area of both tips) level of significance. In the cases of group A, B, C and D, the *t*-Test and *p*-values was ($t(10.3) = 24$, $p = 3\times10^{-10}$, the *t*-Test and *p*-values was ($t(10.3) = 24$, $p = 3\times10^{-10}$, the *t*-Test and *p*-values was ($t(10.3) = 24$, $p = 3\times10^{-10}$ and the *t*-Test and *p*-values was ($t(10.3) = 24$, $p = 3\times10^{-10}$, respectively. Based on the data analysis, the model was found to be suitable for dimensional accuracy (geometry variation) with the linear regression model *p*-value less than 0.05 and lack of fit more than 0.05. Since the linear regression model *p*-value of all the normality plots is found to be above 0.05, it signifies that residue or errors follow the normal distribution.

The average weight of printed parts was 1.3483 g (group A), 1.3195 g (group B), 1.3484 g (group C) and 1.3597 g (group D). The maximum and minimum weight was 1.3597 g (brim with top/bottom thickness) and 1.3195 g (skirt with top/bottom thickness), respectively. The standard deviation of the average weight was ±0.0172 g. Therefore, the average density of PLA Plus printed parts was 1.1878 g/cm^3 with maximum and minimum value of 1.2000 g/cm^3 and 1.1743 g/cm^3, respectively, (for group A, see Figure 18(a)), 1.1641 g/cm^3 with maximum and minimum value of 1.1791 g/cm^3 and 1.1483 g/cm^3, respectively, (for group B, see Figure 18(b)), 1.1794 g/cm^3 with maximum and minimum value of 1.2106 g/cm^3 and 1.1386 g/cm^3, respectively, (for group C, see Figure 18(c)) and 1.1910 g/cm^3 with maximum and minimum value of 1.2058 g/cm^3 and 1.1744 g/cm^3, respectively, (for group D, see Figure 18(d)). Moreover, the reduction in densities were 0.0257 g/cm^3 (for group A), 0.0308 g/cm^3 (for group B), 0.072 g/cm^3 (for group C) and 0.0314 g/cm^3 (for group D). The reduction in densities as an overall with an increase the printing speed, *v*, due to the thermoplastic filament material extrusion might not be enough before the printing nozzle travels to the next printing layer or path when printing speed, *v*, is too fast.

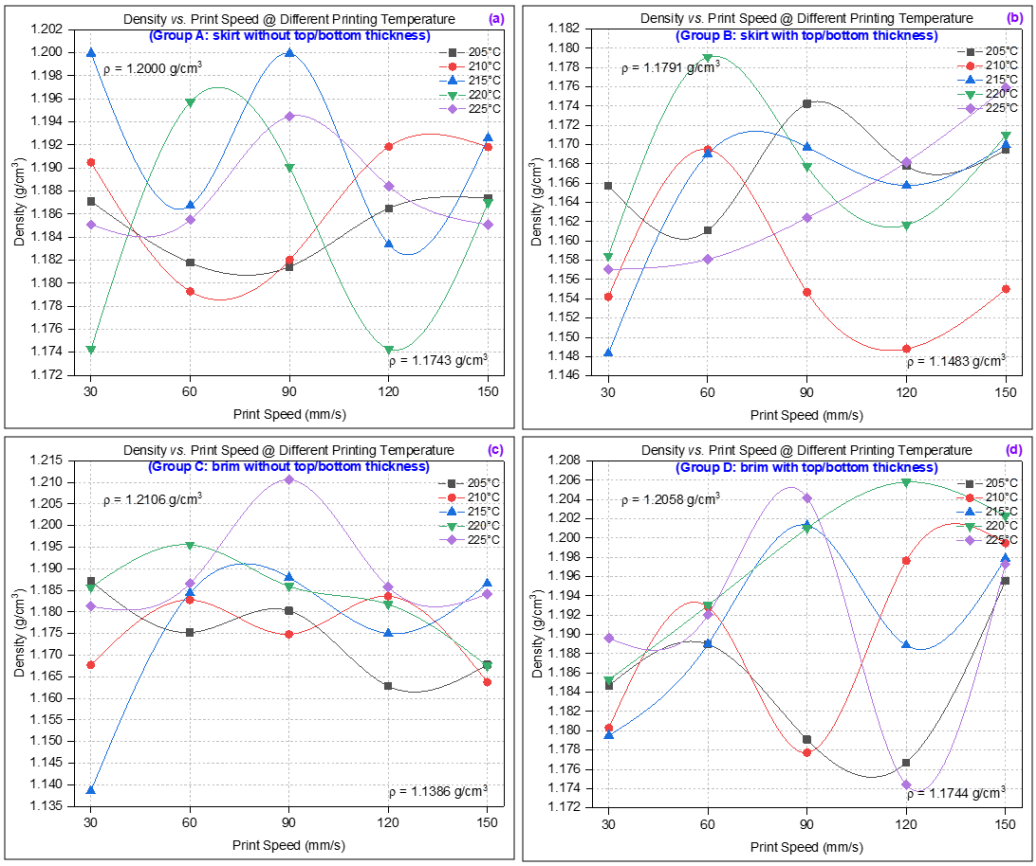

Figure 18. Density versus print speed @ different printing temperature (a) skirt without top/bottom thickness, (b) skirt with top/bottom thickness, (c) brim without top/bottom thickness and (d) brim with a top/bottom thickness

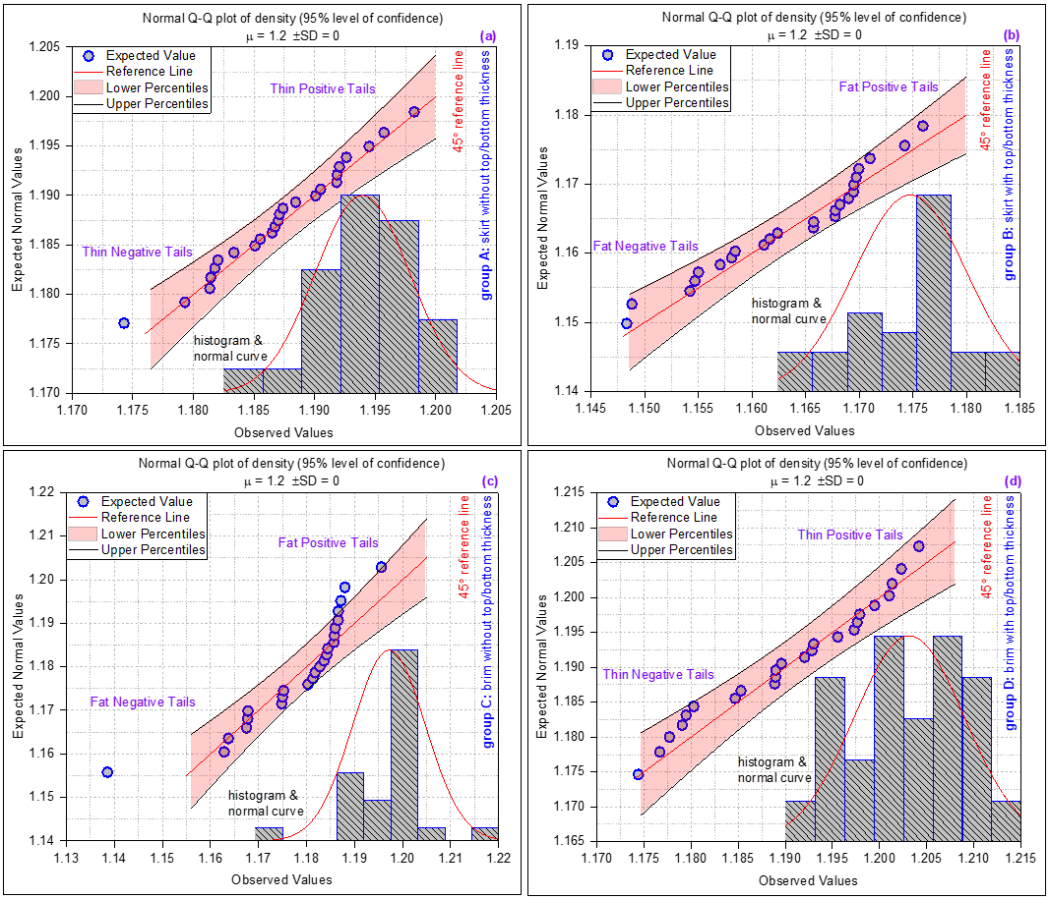

Figure 19. Normal Q-Q (quantile-quantile) plot of density between experimental data and expected data (a) skirt without top/bottom thickness, (b) skirt with top/bottom thickness, (c) brim without top/bottom thickness and (d) brim with a top/bottom thickness

What is more, the maximum and minimum density of the 100 FDM 3D printed samples was 1.1910 g/cm^3 (brim with top/bottom thickness) and 1.1641 g/cm^3 (skirt with top/bottom thickness), respectively. The standard deviation of the average density was ±0.0120 g/cm^3. Based on 3D printing filament specifications, adapted from [38], the density of PLA Plus is around ~1.24 g/cm^3. Therefore, the data results are consistent with the data sheet provided by the manufacturer. Besides, the actual value of the PLA Plus density is not greatly important as long as the Reynold number $Re = \sigma UD/\mu$ is sufficiently low (bellow one) [39]. Based on the data obtained, it is appropriate for fabricating high-quality active implantable medical devices (i.e., drug delivery devices), where the implant weight is essential [40].

The density was decreased from group A (skirt without top/bottom thickness) to group B (skirt with top/bottom thickness) by 0.0237 g/cm^3 whereas, the density was increased from group C (brim without top/bottom thickness) to group D (brim with top/bottom thickness) by 0.0116 g/cm^3. Besides, printed parts with "brim" mode show high density that might be due to incomplete removal of the support materials around the printed part. However, all densities were within the region of around ~1.24 g/cm^3. Finally, brim type as build plate adhesion works perfectly and was very close to the true (recommended) value of the density by almost 97.6% and 97.2% for group C and D, with a coverage factor of $k = 3$, whereas, 96.8% and 95.1% for group A and B, with a coverage factor of $k = 2$.

Figure 19 shows the normal Q-Q (quantile-quantile) plot for density inspection of 100 samples printed by FDM 3D technology with a 95% level of confidence. It can be seen that the blue circles' point in Q-Q plot start on one side of the 45° reference line and they are not quite fully on the opposite side for a long stretch and then move back again to the opposite side of the 45° reference line. This behaviour observed in the Q-Q plot indicated that there is some degree of skewing (skewed right or positive, $R_{sk} > 0$ and that the surface is empty of material, steep peaks and flat valleys).

Figure 19(a) shows almost the Gaussian (normal) distribution compared to another Q-Q plot, whereas the histogram visualizes the data distribution over a certain printed part of the first 25 samples (1 - 25) between 1.170 g/cm^3 and 1.205 g/cm^3 that R generated. The Q-Q plot is drawn with the same data that is displayed in the histogram. The points are much closer to the 45° reference line in the Q-Q plot, indicating that the uniform distribution is a better fit. The Q-Q plot also shows the different phenomenon where there is more concentrated obtained data in the centre of the distribution over the 45° reference line and very small data set in both tails (more likely to be in the left-tailed than right-tailed). Figure 19(b) shows the skewed right distribution or positively, $R_{sk} > 0$, which means that the majority of the obtained data is distributed towards the left side with a long-tailed of obtained data distribution extending out to the right side, whereas the histogram visualizes the data distribution over a certain printed part of the second 25 samples (26 - 50) between 1.145 g/cm^3 and 1.180 g/cm^3 that R generated. The Q-Q plot also shows the obtained data with a fat-tailed distribution, which means that compared to the normal distribution pattern, there is more obtained data set at the excesses of the distribution and less obtained data set in the center of the normal distribution pattern over the 45° reference line. Figure 19(c) shows the skewed right distribution or positively, $R_{sk} > 0$, which means that most of the data is distributed towards the left side with long-tailed data distributions extending out to the right side, whereas the histogram visualizes the data distribution over a certain printed part of the third 25 samples (51 - 75) between 1.130 g/cm^3 and 1.220 g/cm^3 that R generated. The Q-Q plot also shows the obtained data is fat-tailed, which means that compared to the normal distribution there is more stability of data set at the extremes of the distribution and fewer data set in the center of the distribution. Figure 19(d) shows almost the Gaussian (normal) distribution compared to another Q-Q plot, whereas the histogram visualizes the data distribution over a certain printed part of the fourth 25 samples (76 - 100) between 1.170 g/cm^3 and 1.210 g/cm^3 that R generated. The Q-Q plot also shows a different phenomenon where there is more concentrated obtained data set in the centre of the normal distribution pattern over the 45° reference line and very small data set in both tails (left-tailed and right-tailed).

4. Concluding Remarks

The end-user information is crucial to establish precisely the exact geometric with acceptable tolerance ranges and surface quality that the FDM 3D printer can offer. In this paper, the geometry, surface roughness and density of 100 FDM 3D printed parts were comprehensively measured and assessed and the following conclusions were drawn:

- The geometrical accuracy is mainly affected by both printing speed and printing temperature particularly at 30 mm/s and 150 mm/s (for printing speed) and 205°C and 225°C (for printing temperature).
- At 30 mm/s printing speed and 215°C printing temperature, the highest R_a reached by 17.19 µm, while at 150 mm/s printing speed and 220°C printing temperature, the lowest R_a reached by 1.08 µm, with almost ~94% improvement in the surface roughness.
- Group C (brim without top/bottom thickness) represents the greatest deviation by almost ~5.859% while group B (skirt without top/bottom thickness) represents the lowest deviation by almost ~2.29%, for length, width and height variation.
- The relative error of group C > relative error of group D > relative error of group A > relative error of group B.
- Despite the smaller layer height of 40 µm used for part fabrication in low-cost FDM 3D machine, the FDM 3D printed parts demonstrated orientation-dependent geometrical accuracy and density.
- The density was decreased from group A (skirt without top/bottom thickness) to group B (skirt with top/bottom thickness) by 0.0237 g/cm^3.
- The density was increased from group C (brim without top/bottom thickness) to group D (brim with top/bottom thickness) by 0.0116 g/cm^3.

- Density variation among all FDM 3D printed parts was minor, especially when making 100% full-density prints.
- The Q-Q plot indicated that there is some degree of skewing (skewed right or positive, $R_{sk} > 0$, the surface is empty of material, steep peaks and flat valleys).

Conflicts of Interest

The authors declare that there is no conflict of interest involved during the preparation of this manuscript.

Funding Source

The authors received no financial support for the research and/or for the publication of this article.

Availability of Data and Materials

The data analyzed for this manuscript is the part of our research work and is available for public users.

References

[1] Ben-Ner, A. and E. Siemsen, Decentralization and Localization of Production: The Organizational and Economic Consequences of Additive Manufacturing (3D Printing). California Management Review, 2017. 59(2): p. 5-23.

[2] Fafenrot, S., et al., Three-Dimensional (3D) Printing of Polymer-Metal Hybrid Materials by Fused Deposition Modeling. Materials (Basel, Switzerland), 2017. 10(10): p. 1199.

[3] Duarte, L.C., et al., 3D printing of microfluidic devices with embedded sensing electrodes for generating and measuring the size of microdroplets based on contactless conductivity detection. Sensors and Actuators B: Chemical, 2017. 251: p. 427-432.

[4] Mohamed, O.A., S.H. Masood, and J.L. Bhowmik, Mathematical modeling and FDM process parameters optimization using response surface methodology based on Q-optimal design. Applied Mathematical Modelling, 2016. 40(23): p. 10052-10073.

[5] Mostafa, M.A.G., M.S. Alsoufi, and B.A. Tayeb, CAD/CAM Integration Based on Machining Features for Prismatic Parts. International Journal of Emerging Trends & Technology in Computer Science 2015. 4(3): p. 106-110.

[6] Masood, S.H., 10.01 - Introduction to Advances in Additive Manufacturing and Tooling, in Comprehensive Materials Processing, S. Hashmi, et al., Editors. 2014, Elsevier: Oxford. p. 1-2.

[7] Galantucci, L.M., F. Lavecchia, and G. Percoco, Experimental study aiming to enhance the surface finish of fused deposition modeled parts. CIRP Annals - Manufacturing Technology, 2009. 58(1): p. 189-192.

[8] Melchels, F.P.W., et al., Additive manufacturing of tissues and organs. Progress in Polymer Science, 2012. 37(8): p. 1079-1104.

[9] Ryan, I. and B.W. Christopher, Design and manufacture of a Formula SAE intake system using fused deposition modeling and fiber-reinforced composite materials. Rapid Prototyping Journal, 2010. 16(3): p. 174-179.

[10] Vandenbroucke, B. and J.P. Kruth, Selective laser melting of biocompatible metals for rapid manufacturing of medical parts. Rapid Prototyping Journal, 2007. 13(4): p. 196-203.

[11] Lim, S., et al., Developments in construction-scale additive manufacturing processes. Automation in Construction, 2012. 21: p. 262-268.

[12] Bourell, D.L., Perspectives on Additive Manufacturing. Annual Review of Materials Research, 2016. 46(1): p. 1-18.

[13] Zein, I., et al., Fused deposition modeling of novel scaffold architectures for tissue engineering applications. Biomaterials, 2002. 23(4): p. 1169-1185.

[14] Levy, G.N., R. Schindel, and J.P. Kruth, Rapid Manufacturing and Rapid Tooling with Layer Manufacturing (LM) Technologies, State Of The Art and Future Perspectives. CIRP Annals, 2003. 52(2): p. 589-609.

[15] Mueller, B. and D. Kochan, Laminated object manufacturing for rapid tooling and patternmaking in foundry industry. Computers in Industry, 1999. 39(1): p. 47-53.

[16] Evans, J.R.G. and M.J. Edirisinghe, Solid freeform fabrication of ceramics AU - Tay, B. Y. International Materials Reviews, 2003. 48(6): p. 341-370.

[17] Ravi, G.A., et al., Direct laser fabrication of three dimensional components using SC420 stainless steel. Materials & Design, 2013. 47: p. 731-736.

[18] Alsoufi, M.S. and A.E. Elsayed, How Surface Roughness Performance of Printed Parts Manufactured by Desktop FDM 3D Printer with PLA+ is Influenced by Measuring Direction. American Journal of Mechanical Engineering, 2017. 5(5): p. 211-222.

[19] Alsoufi, M.S. and A.E. Elsayed, Quantitative analysis of 0% infill density surface profile of printed part fabricated by personal FDM 3D printer International Journal of Engineering & Technology, 2018. 7(1): p. 44-52.

[20] Alsoufi, M.S. and A.E. Elsayed, Surface Roughness Quality and Dimensional Accuracy - A Comprehensive Analysis of 100% Infill Printed Parts Fabricated by a Personal/Desktop Cost-Effective FDM 3D Printer Materials Sciences and Applications, 2018. 9(1): p. 11-40.

[21] Alsoufi, M.S. and A.E. Elsyeed, Warping Deformation of Desktop 3D Printed Parts Manufactured by Open Source Fused Deposition Modeling (FDM) System. International Journal of Mechanical and Mechatronics Engineering, 2017. 17(4): p. 7-16.

[22] Alsoufi, M.S., et al., Experimental Characterization of the Influence of Nozzle Temperature in FDM 3D Printed Pure PLA and Advanced PLA+. American Journal of Mechanical Engineering, 2019. 7(2): p. 45-60.

[23] Aliheidari, N., et al., Fracture resistance measurement of fused deposition modeling 3D printed polymers. Polymer Testing, 2017. 60: p. 94-101.

[24] Abdullah, A.M., et al., Mechanical and physical properties of highly ZrO2 /β-TCP filled polyamide 12 prepared via fused deposition modelling (FDM) 3D printer for potential craniofacial reconstruction application. Materials Letters, 2017. 189: p. 307-309.

[25] Sun, J., et al., Extrusion-based food printing for digitalized food design and nutrition control. Journal of Food Engineering, 2018. 220: p. 1-11.

[26] Alhijjaj, M., P. Belton, and S. Qi, An investigation into the use of polymer blends to improve the printability of and regulate drug release from pharmaceutical solid dispersions prepared via fused deposition modeling (FDM) 3D printing. European Journal of Pharmaceutics and Biopharmaceutics, 2016. 108: p. 111-125.

[27] Parandoush, P. and D. Lin, A review on additive manufacturing of polymer-fiber composites. Composite Structures, 2017. 182: p. 36-53.

[28] McCullough, E.J. and V.K. Yadavalli, Surface modification of fused deposition modeling ABS to enable rapid prototyping of biomedical microdevices. Journal of Materials Processing Technology, 2013. 213(6): p. 947-954.

[29] Mohan, N., et al., A review on composite materials and process parameters optimisation for the fused deposition modelling process. Virtual and Physical Prototyping, 2017. 12(1): p. 47-59.

[30] Kai, C.C., L.K. Fai, and L. Chu-Sing, Rapid prototyping: principles and applications. 2nd edition ed. 2003, Singapore: World Scientific Publishing Co. Pte. Ltd. 448 pages.

[31] Prusa, J. Prusa Research. 2019 [cited 2019 13/03].

[32] Sood, A.K., R.K. Ohdar, and S.S. Mahapatra, Improving dimensional accuracy of Fused Deposition Modelling processed part using grey Taguchi method. Materials & Design, 2009. 30(10): p. 4243-4252.

[33] Boschetto, A., V. Giordano, and F. Veniali, Modelling micro geometrical profiles in fused deposition process. The International Journal of Advanced Manufacturing Technology, 2012. 61(9): p. 945-956.

[34] Ahn, D., et al., Representation of surface roughness in fused deposition modeling. Journal of Materials Processing Technology, 2009. 209(15): p. 5593-5600.
[35] Nuñez, P.J., et al., Dimensional and Surface Texture Characterization in Fused Deposition Modelling (FDM) with ABS plus. Procedia Engineering, 2015. 132: p. 856-863.
[36] Lee, J.-Y., J. An, and C.K. Chua, Fundamentals and applications of 3D printing for novel materials. Applied Materials Today, 2017. 7: p. 120-133.
[37] ISO4287, Geometrical Product Specifications (GPS) -- Surface texture: Profile method -- Terms, definitions and surface texture parameters. 1997, ISO.
[38] [Online]. Available: http://www.esunchina.net. [Accessed February 2, 2019].
[39] Comminal, R., et al., Numerical modeling of the strand deposition flow in extrusion-based additive manufacturing. Additive Manufacturing, 2018. 20: p. 68-76.
[40] Wolszczak, P., et al., Heat distribution in material during fused deposition modelling. Rapid Prototyping Journal, 2018. 24(3): p. 615-622.